Deep-Sea Research II 58 (2011) 2613–2635

Contents lists available at SciVerse ScienceDirect

Deep-Sea Research II

journal homepage: www.elsevier.com/locate/dsr2

Direct observation of increasing CO_2 in the Weddell Gyre along the Prime Meridian during 1973–2008

Steven M.A.C. van Heuven [a,*], Mario Hoppema [b], Oliver Huhn [c], Hans A. Slagter [a], Hein J.W. de Baar [a,d]

[a] University of Groningen, The Netherlands
[b] Alfred Wegener Institute for Polar and Marine Research, Bremerhaven, Germany
[c] University of Bremen, Germany
[d] Royal Netherlands Institute for Sea Research, Texel, The Netherlands

ARTICLE INFO

Available online 1 September 2011

Keywords:
Southern Ocean
Weddell Gyre
CO_2 uptake
C_{ant}
Weddell Sea Bottom Water (WSBW)

ABSTRACT

The World Ocean takes up a large portion of the anthropogenic CO_2 emitted into the atmosphere. Determining the resulting increase in dissolved inorganic carbon (C_T, expressed in μmol kg^{-1}) is challenging, particularly in the sub-surface and deep Southern Ocean where the time rate of change of C_T (in μmol kg^{-1} $decade^{-1}$) is commonly expected to be low. We present a determination of this time trend of C_T in a dataset of measurements that spans 35 years comprising 10 cruises in the 1973–2008 period along the 0°-meridian in the Weddell Gyre. The inclusion of many cruises aims to generate results that are more robust than may be obtained by taking the difference between only one pair of cruises, each of which may suffer from errors in accuracy. To further improve consistency between cruises, data were adjusted in order to obtain time-invariant values of C_T (and other relevant parameters) over the 35 years in the least ventilated local water body, this comprising the deeper Warm Deep Water (WDW) and upper Weddell Sea Deep Water (WSDW). It is assumed that this normalization procedure will allow trends in C_T in the more intensely ventilated water masses to be more clearly observed.

Time trends were determined directly in measurements of C_T, and alternatively in back-calculated values of preformed C_T (C_T^0; i.e., the C_T of the water at the time that it lost contact with the atmosphere). The determined time trends may be attributed to a combination of natural variability (in hydrography or biogeochemistry) and increased uptake of anthropogenic CO_2 from the atmosphere. In order to separate these natural and anthropogenic components, an analysis of the residuals of a multivariate linear regression (MLR), involving the complete time series of all 10 cruises, was additionally performed. This approach is referred to as the Time Series Residuals (TSR) approach.

Using the direct method, the time trends of C_T in the WSDW are quite small and non-significant at $+0.176 \pm 0.321$ μmol kg^{-1} $decade^{-1}$. On the other hand, the measured concentration of C_T in the Weddell Sea Bottom Water (WSBW) is shown to rise slowly but significantly over the period from 1973 to 2008 at a rate of $+1.151 \pm 0.563$ μmol kg^{-1} $decade^{-1}$. The spatial distribution of these determined increases of C_T in the deep Weddell Gyre closely resembles that of the increase of the anthropogenic tracer CFC-12, this strong similarity supporting a mostly anthropogenic cause for the increasing trend of C_T. Time trends in back-calculated values of C_T^0 appear to be obscured due to uncertainties in the measurements of O_2. Finally, the shallow waters (<200 m depth) do not allow for interpretation since these are strongly affected by seasonality.

Due to the small time trend signal in the WSBW, the TSR approach does not allow for unambiguous attribution of the observed trend in C_T in the WSBW. The residuals of the TSR method do exhibit a time trend (considered representative of the time trend of C_{ant}) of $+0.445 \pm 0.405$ μmol kg^{-1} $decade^{-1}$ (i.e., only 38% of the direct observed time trend in C_T) thus only partly supporting the attribution of the measured time trend of C_T to uptake of anthropogenic CO_2. Another TSR-derived result suggests that there is no significant time trend of biogeochemical changes. A time trend in hydrography of mixing between two deep water masses does exist, as evidenced by a slight positive time trend in the temperature of the WSBW, but is inadequate to explain the time trend of C_T.

After all, the time trend in measured C_T is most straightforwardly ascribed entirely to uptake of C_{ant}, and assuming an exponentially growing history of storage, the observed increase of C_T in the WSBW

* Correspondence to: Centre for Isotope Research, University of Groningen, Nijenborgh 4, 9747 AG Groningen, The Netherlands. Tel.: +31 50 363 4760; fax: +31 50 363 4738.
E-mail address: svheuven@gmail.com (S.M.A.C. van Heuven).

doi:10.1016/j.dsr2.2011.08.007

suggests that a total amount of C_{ant} of 6 ± 3 μmol kg^{-1} has accumulated in this water mass between the onset of the Industrial Revolution and 1995. Extrapolating the determined time trend, the rate of storage of C_{ant} in the deep Weddell Gyre (> 3000 m, west of 20°E) is calculated to be about 12 ± 6 TgC yr^{-1} over the 1973–2008 period. This rate of storage is likely somewhat lower than the rate of export of C_{ant} from the surface water into the deep Weddell Gyre, this due to continuous loss of C_{ant} with WSDW flowing out of the Weddell Gyre into the deep basins of the other oceans as AABW.

1. Introduction and outline

1.1. Introduction

Since the onset of the Industrial Revolution around 1780, the combustion of fossil fuels has led to increasing concentrations of CO_2 in the atmosphere. In 1957 the now world famous time series of atmospheric CO_2 measurements at Mauna Loa, Hawaii was started (Keeling, 1960). After a few years, a rise in CO_2 was apparent, and already in the early 1960s it was recognized that the steady increase was attributable to the burning of fossil fuels. Moreover, it was realized that a portion of the fossil fuel CO_2 would enter into the ocean. Postma (1964) suggested that this invasion of anthropogenic CO_2 into the oceans can in principle be quantified. However, at the time, the analytical precision was inadequate to distinguish within the measured dissolved inorganic carbon (DIC, hereafter C_T; in μmol kg^{-1}), the small anthropogenic (or 'excess') component (C_{ant}; in μmol kg^{-1}) from the large and variable natural background.

The extensive and at the time state-of-the-art dataset for C_T and alkalinity collected during the GEOSECS expeditions in the 1970s (Bainbridge, 1981) led to renewed efforts to quantify C_{ant} in the oceans (Brewer, 1978; Chen and Millero, 1979). Although their approach worked quite well for certain water masses, it was deemed unsuitable for worldwide application. Additionally, at the time the quality of the data was still only modest. Nevertheless, Chen (1993) did produce an estimate of the global ocean inventory (in PgC, equal to 10^{15} g of C) of anthropogenic CO_2 in the year 1980.

The next major improvement was the ΔC^* approach (Gruber et al., 1996) that in combination with the higher accuracy TTO dataset (Transient Tracers in the Ocean, 1981), led to improved estimate of C_{ant} and its corresponding inventory in the North Atlantic Ocean. In the early 1990s, the introduction of certified reference material for C_T (CRM; Dickson, 2001) as well as detailed measurement protocols (Dickson, 1993, updated in 2007), were other major steps forward in accuracy. New high quality datasets of the world oceans, obtained by the WOCE/JGOFS programs, in combination with the ΔC^* approach, led to the first high accuracy estimate of the inventory of C_{ant} of the world oceans (Sabine et al., 2004).

Consensus now exists concerning the inventory of C_{ant} for most of the world ocean. However, the determination of the inventory of C_{ant} in the Southern Ocean remains a challenge, largely because the validity for the application in the Southern Ocean of the various approaches to derive C_{ant} is debatable. Vázquez-Rodríguez et al. (2009) clearly demonstrate the large range in estimates of C_{ant} in the South Atlantic Ocean that are produced by the various approaches. For the deep and bottom water masses, Vázquez-Rodríguez et al. (2009), show these estimates of C_{ant} to range from negligible to values as high as one-third of the concentrations in the surface water.

This study aims to determine the rate of increase of actually measured C_T over 35 yr (1973–2008) in the Weddell Gyre using ocean interior data from 10 successive cruises. In the little-ventilated (or 'old') lower Warm Deep Water (WDW) and upper WSDW, no time trend of C_T is expected or observed, therefore all cruise datasets are normalized to a common level in this water body. Next, the normalized C_T is gridded. From these grids, the spatial distribution along the section (55°S–70°S) of the generally increasing time trend of C_T is obtained, with striking resemblance to the similar distribution of time trends in the independent anthropogenic transient tracer chlorofluorocarbon-12 (CFC-12). Moreover, for two individual key water masses (the Weddell Sea Deep Water (WSDW) and Weddell Sea Bottom Water (WSBW)) the time trend of C_T (in μmol kg^{-1} decade^{-1}) is calculated, from which a new improved estimate of the C_{ant} and its inventory in Weddell Gyre is reported. Obviously, the time trend of C_T may partly be due to natural variability of water mass mixing and biogeochemistry. Any effect of water mass mixing is assessed in a simple mixing model, relying on observed temperature trends. Moreover, the novel Time Series Residuals (TSR) method is designed to extract the sought after increase of anthropogenic C_{ant} and distinguish this from the natural variability. The novel TSR method relies on the measured C_T and a suite of independent ancillary measured variables of all 10 cruises.

Several stations of the 1973 GEOSECS expedition comprised the first suitable observations along the Prime Meridian in the Weddell Gyre. Since then, this hydrographic section along the 0°-meridian has been (more or less extensively) occupied by at least another 9 expeditions that performed high-quality measurements of C_T and additional relevant oceanic properties, (Tables 2 and 3). To the best of our knowledge this is the longest existing ocean section time series of C_T data. Therefore this is a uniquely promising section for assessing the rate of increase of C_T. Moreover it serves as a field test of the novel TSR approach for extracting the increasing C_{ant} signal from noise due to natural variability. On the other hand the Southern Ocean south of 50°S is often considered to feature only low concentrations of anthropogenic carbon (e.g., Sabine et al., 1999; Hoppema et al., 2001; but see Lo Monaco et al., 2005a, 2005b). This conceivably constitutes a challenge for the demonstration of the direct C_T time trend and the TSR approach for discerning C_{ant}. However in the coming decades, and already in regions with a higher rate of increase (notably the North Atlantic Ocean; Pérez et al., 2008, 2010; Olafsson et al., 2009; Peng and Wanninkhof, 2010), both the direct C_T time trend approach and the Time Series Residuals method are expected to deliver a strong signal of increasing C_T and increasing C_{ant}, respectively.

1.2. Outline

After a brief introduction of the unique hydrography of the Weddell Gyre (Section 2), we will discuss in more detail the preceding concepts and approaches for quantifying the invasion of anthropogenic CO_2 into the oceans (Section 3). Firstly, five different published original approaches for determining the **total inventory** of C_{ant} in the ocean interior are recognized, and discussed with regard to assumptions and uncertainties, notably for the Southern Ocean (Section 3.1). Secondly, we mention three approaches for quantifying the **change** of such C_{ant} (i.e., ΔC_{ant}) between two successive cruises along one and the same transect (Section 3.2). Thirdly we introduce the novel Time Series Residuals (TSR) approach for extracting from a suite of several cruises along one transect the **rate of increase** of C_{ant} (Section 3.3).

Next, in text Sections 4 through 7, both the direct C_T time trend method and the TSR approach are applied to the suite of 10 cruises over 35 yr along the Prime Meridian transect in the Weddell Gyre, aiming to establish the rate of increase of C_T and C_{ant}, respectively.

2. Hydrography

The Southern Ocean comprises all waters south of the Subtropical Front situated at about 40°S, while the Antarctic Ocean proper comprises all waters south of the Polar Front situated at about 50°S (Deacon, 1984). The hydrography of the Antarctic Ocean is dominated by the wind-driven Antarctic Circumpolar Current (ACC), which flows relatively unhindered around Antarctica at all depths (Fig. 1). The eastward flows of wind and ocean currents also drive the Weddell Gyre, which rotates cyclonically (i.e., clockwise) between the Antarctic continent to the south, the Antarctic Peninsula to the west and the ACC to the north and east. The eastern-most extension of the Weddell Gyre is located at 25–30°E. Several water masses flow into and out of the ACC and the Weddell Gyre (Fig. 2). From the north, at depths below about 1500 m, North Atlantic Deep Water (NADW) mixes into the ACC. However, before reaching the ACC, as well as within it, the NADW is deflected upward by the denser Antarctic Bottom Water (AABW) from the south, which wedges itself underneath the NADW. In the ACC there is large-scale mixing of several water masses including the NADW, resulting in a relatively homogeneous water mass called Circumpolar Deep Water (CDW). South of the ACC, the shallowing CDW penetrates southward toward the Antarctic continent at a depth of about 250–750 m. Being distinctly warmer (potential temperature $(\theta) > 0$ °C, see Table 2 for definitions) and saltier than the overlying, frigid and fresh polar water masses, it is locally referred to as Warm Deep Water (WDW). Strong and continuous circumpolar westerly winds cause upwelling of the WDW at latitudes between 60°S and 65°S in the Weddell Gyre. The upwelled waters are subsequently redistributed. A small fraction flows southward, replenishing the downwelling waters near the continent. A larger fraction flows northward where, between 50°S and 45°S, it subducts to depths of about 1000 m, and subsequently flows toward the equator as Antarctic Intermediate Water (AAIW).

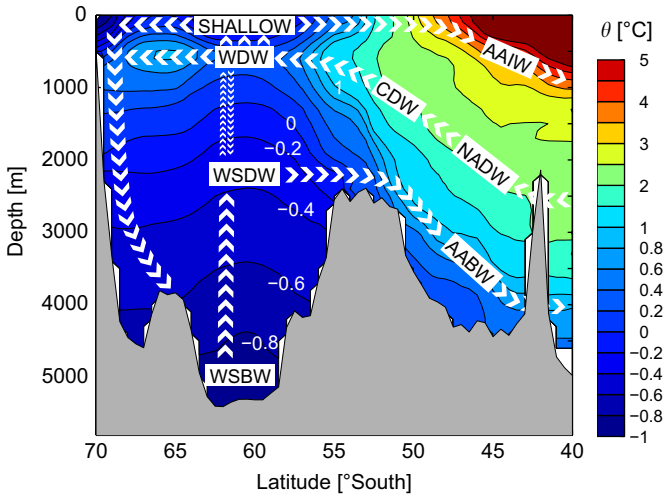

Fig. 2. Section along the 0°-meridian in the Southern Ocean showing potential temperature (θ) (°C) and the generalized locations and movements of various water masses. The ~45°S to ~55°S region represents the Antarctic Circumpolar Current. The 55°S–70°S region represents the actual Weddell Gyre, subject of this study. AAIW=Antarctic Intermediate Water; NADW=North Atlantic Deep Water; CDW=Circumpolar Deep Water; AABW=Antarctic Bottom Water; SHALLOW=the shallowest 200 m of the water column; WDW=Warm Deep Water; WSDW=Weddell Sea Deep Water; WSBW=Weddell Sea Bottom Water.

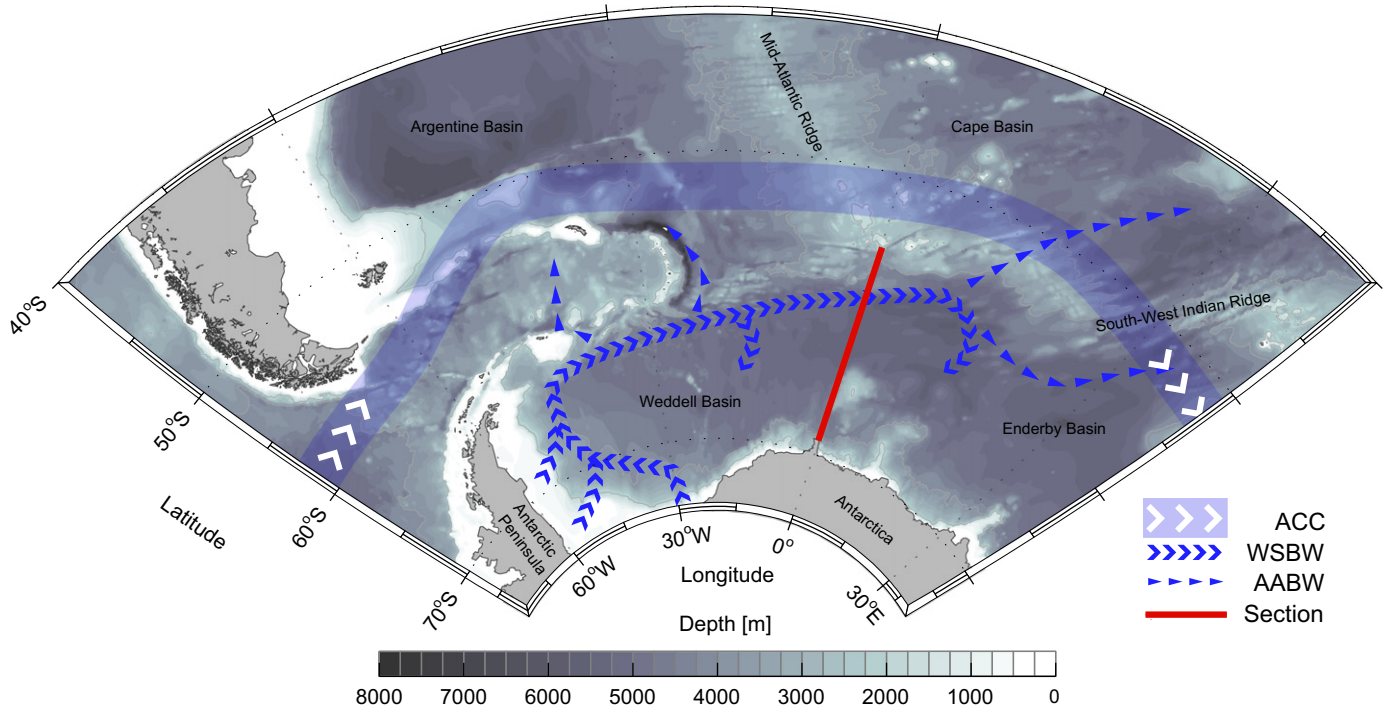

Fig. 1. Chart of the Weddell Basin and its surroundings, indicating the extent of the Weddell Gyre to about 30°E, the generalized course of the Antarctic Circumpolar Current (ACC; blue shaded with white chevrons) and the pathways of the of the WSBW (blue chevrons) and AABW (blue triangles). The formation areas of WSBW are situated at the southwestern perimeter of the Weddell Basin. Also shown is the general location of the oceanographic research section along the 0°-meridian.

The AABW, spilling from the intermediate and deep depths of the Weddell Basin over and through the Mid-Atlantic Ridge (MAR) and the South–West Indian Ridge (SWIR), flows northward into the South Atlantic and South Indian basins (Fig. 1). In the Weddell Basin, the pool of AABW (locally referred to as Weddell Sea Deep Water, WSDW) is replenished from below, by formation of dense water at sites along the edge of the Antarctic continent and the ice shelves of the Weddell Sea. The dense water flows downslope, entraining significant amounts of WDW, and accumulates near the bottom or at depths according to the density it achieves. This continuous supply of cold ($\theta < -0.7$ °C) water – referred to as Weddell Sea Bottom Water (WSBW) – forces the near-bottom pool to extend upward where it is mixed into the overlying water (Foster and Carmack, 1976; Klatt et al., 2005). Typical features of the surface water at the margin of the Weddell Sea (i.e., relatively low temperature, salinity, nutrients and C_T; high oxygen and CFCs) are retained during its transfer to depth. The characteristics of the WDW, the water mass that influences the intermediate depth Weddell Gyre from above, are diametrically opposed to this, and the resulting mixing gradients are clearly distinguishable for these properties. The intermediate state between WDW and WSBW, generally between 2000 and 4000 m depth, constitutes the WSDW, and is the main source of AABW. This study is restricted to the sub-surface water masses within the Weddell Sea: WDW, WSDW and WSBW.

Much of the uncertainty about the inventory of C_{ant} of the Antarctic Ocean stems from this unique local hydrography. In the North Atlantic and Arctic oceans, deep water formation is generally thought to result from deep convection of cool, dense surface waters in wintertime. These waters have been cooled during extensive contact with the overlying atmosphere, meanwhile also exchanging gases such as CFCs, O_2 and CO_2. Deep water formation in the Weddell Sea on the other hand, largely takes place along the Antarctic continent, under strong influence of ice-shelves (i.e., often preventing direct air/sea gas exchange). The waters contributing to the nascent deep water generally have only recently upwelled. The unknown and likely variable degree to which they equilibrate with the atmosphere before reaching the ice-shelf zones, makes their ability to sequester anthropogenic CO_2 difficult to predict or quantify.

3. Concepts and approaches to derive C_{ant} and its change in the ocean interior

Firstly, five different published original approaches for determining the **total inventory** of C_{ant} in the ocean interior (Section 3.1) are recognized, and discussed with regards to assumptions and uncertainties, notably for the Southern Ocean. Secondly, we mention three approaches for quantifying merely the **change** of such C_{ant} (i.e., ΔC_{ant}) between two successive cruises along one and the same transect (Section 3.2). Thirdly we introduce our novel approach for extracting from a suite of several cruises along one transect the **rate of increase** of C_{ant} (Section 3.3): the Time Series Residuals (TSR) approach. Finally, all three groups of approaches are summarized in Table 1.

3.1. Determination of the concentration of C_{ant} in the ocean interior

3.1.1. C_{ant}: the C_T^0 approach

The gradual uptake by the ocean of anthropogenic CO_2 from the atmosphere is detectable, in principle, as the ensuing gradual rise of C_T at the surface and eventually within the ocean interior. However, the presence and variability of biogeochemical processes in the ocean interior obscure these trends, and may need to be compensated for in order to be able to observe the increasing C_T. Remineralization of organic matter and the dissolution of calcium carbonate ($CaCO_3$) do not only influence C_T but also the concentrations of dissolved oxygen (O_2) and total alkalinity (A_T), respectively. The stoichiometric ratios of these biogeochemical reactions have been shown to be fairly uniform in the oceans (Redfield et al., 1963; Anderson and Sarmiento, 1994). Therefore, by conversely using the changes in O_2 and A_T from their preformed (i.e., at the time a water mass by its subduction loses contact with the atmosphere) values in the original surface water, these biogeochemical effects on C_T can be quantified and subtracted from the measured C_T in the interior ocean. This yields the reconstructed (or 'back-calculated') C_T that a water parcel had at the time of formation at the surface (preformed C_T: C_T^0):

$$C_T^0 = C_T - \psi_{O:C}(\mathrm{AOU}) - 0.5(A_T - A_T^0 + \psi_{O:N}(\mathrm{AOU})) \quad (1)$$

Here, AOU (apparent oxygen utilization) represents the amount of oxygen consumed by remineralization of organic matter. The AOU is defined as the difference between the measured O_2 of an ocean interior water sample and the preformed concentration, O_2^0, which is calculated (following Weiss, 1970) as the dissolved O_2 presumably in equilibrium with atmospheric pO_2, using the measured values of salinity and temperature of the sample. The term $\psi_{O:C}(\mathrm{AOU})$ yields the amount of carbon released (as CO_2) during biological respiration, calculated from the stoichiometry of consumption of O_2 and production of CO_2 ($\psi_{O:C}$), and AOU. The value of preformed A_T (A_T^0) is estimated from conservative properties of a water mass (any one or a combination of θ, S, PO or NO; Broecker, 1974), using relationships determined between the measured A_T and these properties in the formation region of the subducted water mass. The factor of 0.5 here reflects the fact that the dissolution of $CaCO_3$ increases C_T at half the rate at which it increases A_T. The extra term $\psi_{O:N}(\mathrm{AOU})$ corrects the estimate of dissolution of $CaCO_3$ (derived from the change of A_T) for the slight effect on alkalinity of the release of nitrate ion during remineralization of organic matter (Brewer and Goldman, 1976).

In a case study of the AAIW, flowing from its formation region at the Antarctic Polar Front to the low latitude South Atlantic, Brewer (1978) was able to calculate C_T^0 over the 45°S–4°S range, and from this derived the corresponding atmospheric pCO_2 value to decrease from ~300 μatm at 45°S to ~250 μatm between 20°S and the Equator. Taking into account the -30 ± 10 μatm range of the pCO_2 disequilibrium with the atmosphere at the formation region at 50°S, a pre-industrial atmospheric pCO_2 of ~280 μatm was obtained. Similarly, Chen and Millero (1979) reported the gradual increase of oceanic CO_2 for the intermediate depth salinity minimum and the deep temperature minimum along a complete Atlantic section (50°S–50°N).

The C_{ant} of a water sample can be calculated by subtracting from C_T^0 the *pre-industrial* value of C_T^0 ($C_{T,\,preind}^0$; Poisson and Chen, 1987; Körtzinger et al., 1998):

$$C_{ant} = C_T^0 - C_{T,\,preind}^0 \quad (2)$$

The $C_{T,\,preind}^0$ is assumed to be equal (and constant through time) for all samples within a water mass, and is generally obtained from the interior of the water mass under consideration, if that can be determined (from absence of anthropogenic tracers such as tritium or CFCs) to be still uncontaminated with C_{ant} (i.e., $C_{T,\,preind}^0 = C_{T\ interior}^0$). For more shallow water masses, however, even the inner part may have already become contaminated with C_{ant}. For such cases, one needs to resort to calculate $C_{T,\,preind}^0$ using the following equation:

$$C_{T,\,preind}^0 = f(S, T, A_T^0, pCO_{2,\,preind}) \quad (3)$$

where $pCO_{2,\,preind}$ is the assumed pCO_2 of the surface water in pre-industrial times. However, because subducting waters are generally not in equilibrium with the overlying atmosphere

Table 1
A selection of techniques available for the calculation of the concentration of anthropogenic CO_2 (C_{ant}), or the increase therein (ΔC_{ant}), in the ocean. Some of the major perceived strengths and drawbacks of each are given in the table. See further text Section 3.

Technique	Refs.	Comment	Required measurements	Strengths	Assumptions made	Drawbacks/sensitivities
Determining C_{ant}						
C_T^0	Brewer (1978) and Chen and Millero (1979)	Shiller (1981)	O_2, C_T, A_T	Conceptually simple	Surfaces histories of C_{ant}, O_2 and A_T. No diapycnal mixing	Requires pre-industrial reference water mass; hence difficult for worldwide application
ΔC^*	Gruber et al. (1996)	Matsumoto and Gruber (2005)	O_2, C_T, A_T, transient tracer	Reduced sensitivity to some assumptions. No requirement of reference water mass	Surfaces histories of C_{ant}, O_2 and A_T. No diapycnal mixing	Must obtain ventilation age estimate of sample
TTD	Hall (2002)	–	Transient tracer	Independent of biogeochemical data. Inherently allows for mixing	General shape of TTD. Surface histories of CFC and C_{ant}	TTD difficult to infer for certain regions
TrOCA	Touratier and Goyet (2004a, 2004b)	Yool et al. (2010)	O_2, C_T, A_T	Easily implemented	TrOCA^0-parametrization may be extrapolated to higher temperatures	TrOCA^0-parameterization likely not widely valid
TSS	Tanhua et al. (2007)	–	ΔC_{ant} (see below)	Conceptually straightforward	TSS has been reached. Surface history of C_{ant}	Requires ΔC_{ant} of samples
Determining ΔC_{ant}						
Change in C_T	This study (trend)	–	C_T	Uses only high accuracy data ($\pm 0.1\%$)	Biogeochemical noise smaller than ΔC_{ant}	Aliases in hydrographically and biogeochemically dynamic regions
Change in C_T^0	Peng et al. (1998)	–	O_2, C_T, A_T	Insensitive to variable biogeochemistry	Uncertainty of biogeochemical corrections applied are smaller than ΔC_{ant}	Requires use of lower accuracy ancillary data ($\pm 2\%$). Aliases in hydrographically dynamic regions
MLR	Wallace (1995)	Levine et al. (2008)	O_2, C_T, A_T, nutrients	Insensitive to variable hydrography and biogeochemistry	Ancillary data are independent. ΔC_{ant} is linearly representable by ancillary data. No 'secular' trends	Requires use of lower accuracy ancillary data ($\pm 2\%$). Interpretation of results is ambiguous
eMLR	Friis et al. (2005)	Levine et al. (2008)	O_2, C_T, A_T, nutrients	Insensitive to variable hydrography and biogeochemistry	Ancillary data are independent. ΔC_{ant} is linearly representable by ancillary data. No 'secular' trends	Requires use of lower accuracy ancillary data ($\pm 2\%$). Interpretation of results is ambiguous
TSR	This study	–	O_2, C_T, A_T, nutrients	Insensitive to variable hydrography and biogeochemistry. Use of many cruises reduces sensitivity to biases	Ancillary data are independent. ΔC_{ant} is linearly representable by ancillary data. No 'secular' trends	Requires use of lower accuracy ancillary data ($\pm 2\%$)

(Gruber et al., 1996; Takahashi et al., 2009), any assumed value of $pCO_{2,\,preind}$ is debatable, which jeopardizes the application of the C_T^0 approach in shallower, more recently ventilated waters masses. Several additional problems of the C_T^0 approach should be mentioned. The inherent assumption of pO_2 equilibrium (for calculation of AOU) with the atmosphere may be invalid, and is of strong influence on the calculated C_{ant}. For example, in the Southern Ocean the air–sea gas exchange is hampered by ice cover and Lo Monaco et al. (2005a, 2005b) assume a mean undersaturation of 12%, yielding an about 7 μmol kg^{-1} higher C_{ant} in the WSBW than in the case of O_2 equilibrium with the atmosphere. Moreover, the stoichiometric ratio between the consumption of oxygen and production of CO_2 ($\psi_{O:C}$) is not uniform but varies between oceans and depth intervals, significantly affecting the C_{ant} (Wanninkhof et al., 1999). Furthermore, over the years, progressively less of the old waters will remain suitable to serve as pre-industrial reference. Moreover, although the detection of more recently emitted transient tracers (notably CFCs, ^{3}H, ~1950–1960 era) shows a water sample is not pristine anymore, the absence of such tracers does not necessarily imply the absence of C_{ant}, for which emission commenced already at ~1780. Finally, a constant disequilibrium value of pCO_2 between air and sea is assumed, yet in reality this value likely varies over the years (Metzl, 2009).

3.1.2. C_{ant}: the ΔC^* approach

The ΔC^* technique (Gruber et al., 1996) overcomes an important shortcoming of the C_T^0 method in that it allows the pCO_2 disequilibrium in the formation region to be quantified from measurements even for water masses that are contaminated with C_{ant}, provided that the age of the water sample is known. The ΔC^* technique defines C_{ant} as follows:

$$C_{ant} = C_T^0 - C_{eq280} - C_{diseq} \quad (4)$$

The first two terms on the right hand side of Eq. (4) comprise 'ΔC^*' such that:

$$C_{ant} = \Delta C^* - C_{diseq} \quad (5)$$

Here, C_T^0 of the water sample is calculated according to Eq. (1), C_{eq280} is the hypothetical C_T^0 of the water if it were in pCO_2-equilibrium with the pre-industrial atmosphere of 280 μatm (at the S, T and A_T^0 of the sample), and C_{diseq} represents the small difference versus C_{eq280} due to air–sea pCO_2 disequilibrium in the formation area. Because C_{diseq} is not expected to be the same for all water masses, it is generally determined for each of a number of isopycnal intervals (layers of water between distinct lines of equal density).

For the deepest isopycnal intervals, C_{diseq} is obtained by observing ΔC^* versus (generally) latitude. Such a plot shows ΔC^* decreasing from the higher latitude formation regions toward the equator (reflecting the higher C_T in recently ventilated waters) where at some latitude it reaches a baseline level (extending toward the equator) comprising all samples that have a pre-industrial ventilation history. The mean of these pre-industrial samples is taken to represent the mean C_{diseq} of the isopycnal interval. For example, Gruber et al. (1996) show that the deep (>2000 m) water masses in the North Atlantic south of Iceland have a C_{diseq} of about -16 μmol kg^{-1}, corresponding to a ΔpCO_2 of about -32 μatm. This suggests that these waters generally have not completed the process of taking up CO_2 from the atmosphere before they were subducted.

For shallower isopycnal intervals, no such baseline of ΔC^* may be observed, due to the fact that the whole interval is already contaminated with C_{ant}, such that C_T and thereby ΔC^* are elevated above pre-industrial levels. However, with knowledge of the ventilation age of the samples (obtained independently from CFCs, ^{3}H–^{3}He or other transient tracers), an alternative may be calculated for C_{eq280}, that is, a C_{eqt} referenced to the known atmospheric pCO_2 of the year t of formation. For instance, for a sample with ventilation age dating from the year 1990, one would calculate C_{eq353}. Subsequent assessment, over a range of latitudes (or ages), of ΔC^* (now called ΔC_t^*) once again yields a baseline that may be taken to represent C_{diseq}. Gruber et al. (1996) in this manner show that relatively shallow water masses (those originally formed in the seas north of Iceland) exhibit a ΔpCO_2 of about −85 μatm. Once C_{diseq} is determined for each isopycnal interval, the value of C_{ant} is easily calculated using Eq. (5).

Because C_{diseq} is inferred as the mean difference between C_T^0 and C_{eq280} (or C_{eqt}), its value not only represents the effects of the air–sea disequilibrium of pCO_2 at the time of subduction, but also the effects of a conceivable pO_2 disequilibrium (which affects C_T^0). Because C_{diseq} is subtracted from ΔC^* to obtain C_{ant}, any effect on C_{ant} is canceled out. In the same way, C_{diseq} includes the effects of any inaccuracy of the remineralization ratio values $\psi_{O:C}$ and $\psi_{O:N}$ of Eq. (1), which are also canceled out (again through C_T^0), thereby removing another source of uncertainty that is present in the C_T^0 method.

Using the ΔC^* method, Sabine et al. (2004) used interior ocean measurements obtained during WOCE and JGOFS studies of the 1990s to constrain the inventory of C_{ant} of the world ocean to 118 ± 19 PgC in 1994.

Matsumoto and Gruber (2005) assessed the ΔC^* method and realized that biases in its results are introduced by the assumption of constant (over time) C_{diseq} and the simplified derivation of ventilation age from transient tracers (see also Hall et al., 2004). Matsumoto and Gruber (2005) suggest that these two biases can be minimized by (i) varying C_{diseq} as a function of the uptake of C_{ant} itself, and by (ii) taking into account the age spectrum of water when determining ventilation ages, respectively. However, for the Southern Ocean the second suggestion (ii) is notably difficult, because the age spectrum of the locally formed water masses is strongly bimodal (Khatiwala et al., 2001; Hall et al., 2002; Peacock and Maltrud, 2006), and therefore difficult to establish using tracer measurements. Therefore, application to the Southern Ocean of the ΔC^* approach remains challenging.

3.1.3. C_{ant}: the TrOCA approach

Application of the TrOCA approach (Tracer combining Oxygen, Carbon and Alkalinity; Touratier and Goyet, 2004a, 2004b) is more straightforward. The approach requires less variables to be measured (only O_2, C_T, A_T and θ), and avoids the rather complex estimation of air–sea disequilibria for pCO_2. In the TrOCA method, first the effects of remineralization of organic matter and dissolution of calcium carbonate are compensated:

$$\mathrm{TrOCA} = O_2 + 1.2C_T - 0.6A_T \quad (6)$$

The resulting value of TrOCA includes the C_{ant} component. Next, if the pre-industrial TrOCA (TrOCA^0) value of the water sample can be obtained, this C_{ant} component can be calculated:

$$C_{ant} = (\mathrm{TrOCA} - \mathrm{TrOCA}^0)/1.2 \quad (7)$$

For old, deep water masses that have not been in contact with the modern atmosphere, the value of TrOCA^0 is assumed to be equal to TrOCA. In order to obtain values of TrOCA^0 in shallower water masses (ventilated after 1780), the observed relationship in the deep waters of TrOCA and potential temperature (and in subsequent work also A_T; Touratier et al., 2007) is extrapolated to the higher θ of the shallower, warmer, water masses. However, Yool et al. (2010) argue that the extrapolation of a single TrOCA^0-versus-θ relationship toward shallower, warmer waters cannot represent the full range of pO_2- and pCO_2-disequilibria encountered in the different involved formation regions and processes.

Therefore, the TrOCA approach necessarily can likely only be applied on a sub-basin scale. In the deep Southern Ocean, no required pristine water mass exists anymore, as suggested by the fact that anthropogenic CFCs are found at all depths (Klatt et al., 2002), which complicates the derivation of a locally predictive relationship for $TrOCA^0$.

3.1.4. C_{ant}: the Transit Time Distribution (TTD) approach

The Transit Time Distribution approach (TTD; Hall et al., 2002; McNeil et al., 2003; Waugh et al., 2006) relies on a combination of measurements of one or more oceanic anthropogenic transient tracers (e.g., CFCs, SF6), their atmospheric time histories, and hydrographic data to estimate the most likely ventilation age distribution (i.e. the TTD) of water parcels in the ocean interior. The inferred TTDs are then combined with the assumed surface water time history of C_{ant} to calculate the interior ocean concentrations of C_{ant}. Waugh et al. (2006) have used the TTD method to estimate a total inventory of C_{ant} for the global ocean of 94–121 PgC for 1994.

The complete independence of the TTD method from measurements of oceanic C_T makes it a valuable complement to C_T-based approaches. However, like some of the previous approaches, the TTD approach requires assumptions of the time histories of C_{ant} and CFC in the surface ocean, which are strongly dependent on the unknown (and likely variable) time histories of equilibration with the atmosphere. Additionally, as already mentioned in text Section 3.1.2, the shape of the TTD may be difficult to quantify specifically in the Weddell Gyre, where upwelling, subduction and entrainment occur on small temporal and spatial scales. The concurrent measurements of transient tracers with strongly differing atmospheric time histories (e.g., CFC-12 and SF_6; Walker et al., 2000; Tanhua et al., 2008; Fine, 2011) in principle allows for some of the uncertainty of the shape of the TTDs to be resolved. However, no datasets of SF_6 in the Weddell Gyre have been described in the literature yet.

3.1.5. C_{ant}: the Transient Steady State (TSS) approach

Given a sufficiently long time, an exponentially increasing concentration of C_{ant} at the surface of the ocean will result in a similar exponential increase of C_{ant} at depth, the so-called Transient Steady State (TSS; Tanhua et al., 2007). Therefore the *rate of increase* of C_{ant} at any location in the ocean interior is proportional to the *concentration* of C_{ant} (Gammon et al., 1982; Tanhua et al., 2007). This method thus allows the derivation of a value of C_{ant} given only the rate of change of C_{ant}. However, just as for most of the above methods, the finally derived C_{ant} concentration depends strongly on the assumed time history of surface water pCO_2. Nevertheless, this technique will be used in below Section 7.5 to convert the determined rate of increase of C_{ant} in the deep Weddell Sea into an estimate of the total concentration of C_{ant}.

3.2. Determination of the increase ΔC_{ant} between two consecutive cruises

The expected increase of C_T at the ocean surface due to the accumulation of C_{ant} is about 1 μmol kg^{-1} yr^{-1}, against a background concentration in the order of 2000 μmol kg^{-1}. In deeper waters, this increase will be smaller and therefore more difficult to discern against the large background value. Moreover, the signal may be obscured by variability of formation and mixing of deep water masses (Fahrbach et al., 2004) and variability of biological processes (Sabine et al., 2008). We discuss three published approaches for quantifying the increase in C_{ant} (ΔC_{ant}) between two successive cruises along one and the same transect.

3.2.1. ΔC_{ant}: determination of the change in C_T or C_T^0

Early determinations of the increase of C_{ant} between (once) repeated ocean sections were reported by Hoppema et al. (1998) and Peng et al. (1998). The former study in the western Weddell Sea explicitly considered variable formation properties of water masses. The latter study accounted for the confounding effects of variability in such natural processes as water mass mixing and biology, evaluating the increases of C_T^0 along isopycnal surfaces.

3.2.2. ΔC_{ant}: the Multivariate Linear Regression (MLR) approach

Wallace (1995) proposed the use of a Multivariate Linear Regression (MLR) technique to assess the changes in C_{ant} between two subsequent occupations of the same ocean station or section. The technique correlates measured values of C_T with a suite of ancillary tracers in order to determine these changes, while accounting for some of the variability in hydrographic conditions and biological activity.

Firstly, for one single cruise, a mathematical relationship is derived between the measured C_T and the values of ancillary physical and biogeochemical properties that are known to be related to the natural sub-surface variability of C_T. These properties (generally θ, S, one or more nutrients, O_2 or AOU and A_T) are independent of increasing C_{ant}, but represent the natural processes affecting C_T: the mixing of water masses, remineralization of organic matter and dissolution of $CaCO_3$. The approach does not require knowledge about remineralization ratios or mixing processes. The derived MLR is used to predict the values C_T^{MLR}, and by comparison with the actually measured C_T values, the residuals ($C_{residual,1}^{MLR}$) are obtained. In practice, these residuals are normally distributed around zero, with a typical standard deviation in the order of 4 μmol kg^{-1}. Subsequently, for a second cruise some years later, the MLR relationship of the first cruise is combined with the ancillary values of the second cruise, to derive $C_{residual,2}^{MLR}$. Finally, by comparison of the depth profiles of $C_{residual,1}^{MLR}$ and $C_{residual,2}^{MLR}$ the apparent increase ΔC_{ant} is derived.

Application in the Indian Ocean by Sabine et al. (1999) resulted in an estimate of the increase of C_{ant} in the Indian Ocean north of 35°S. McNeil and coworkers used this technique to demonstrate the invasion of both C_{ant} and the $\Delta^{13}C_T$-signal into the Southern Ocean south of Australia (McNeil et al., 2001). Peng et al. (2003) reported an increase of anthropogenic CO_2 in the Pacific Ocean over two decades. Matear and McNeil (2003) found reasonable agreement between the MLR-method and the TTD technique (Section 3.1.4) in the Southern Ocean.

3.2.3. ΔC_{ant}: the Extended Multivariate Linear Regression (eMLR) approach

In the original MLR approach (Section 3.2.2), the derived ΔC_{ant} is affected by errors of both the suite of ancillary measurements and the measured C_T values. The extended MLR (eMLR; Friis et al., 2005) aims to minimize the effect of the errors of the ancillary measurement. Here one derives, again using MLR, a unique relationship for each of two cruises and uses the difference between the coefficients of the two relationships as a predictor of ΔC_{ant} between the cruises. The eMLR approach has been applied by several investigators (e.g., Olsen et al., 2006; Tanhua et al., 2007; Sabine et al., 2008; Hauck et al., 2010). The approach is deemed less sensitive than the original MLR-method to systematic errors (biases) in the ancillary data of each cruise. Nevertheless, the sensitivity of the results to biases in the measurements of C_T of either involved cruise remains. This jeopardizes the application of this method, notably in the Weddell Gyre where time trends in C_{ant} are deemed to be small.

Every technique used to determine anthropogenic changes in C_T between two cruises is sensitive to biases in the data of either

cruise. Such biases are not uncommon: before the introduction of certified reference material (CRM: Dickson, 2001), analytical biases in C_T and A_T could be more than 10 μmol kg^{-1} (Stoll et al., 1993). Even today, now that values of C_T and A_T are more accurate, the measurements of dissolved nutrients and oxygen occasionally remain inaccurate by several percent. Dataset synthesis efforts like GLODAP (Key et al., 2004) and CARINA (Key et al., 2010) aim to identify and remove these biases (Tanhua et al., 2010), but the resulting datasets are obviously not as good as what could analytically have been achieved at the time, or can be achieved nowadays. Until primary measurements of required ancillary parameters reach a level of accuracy comparable to that attained in the measurements of C_T and A_T themselves, the interpretation of results of the back-calculations and MLR-type methodology will be ambiguous to some extent. Moreover, Levine et al. (2008) argue and illustrate that the (e)MLR approaches do not necessarily yield accurate results in the presence of trends in the ancillary data that persist over the period of interest (so-called *secular trends*). The warming of shallow water masses due to global warming is a case in point.

3.3. The Time Series Residuals (TSR) approach for multiple repeat cruises along one transect

Here we introduce an approach for extracting from a suite of multiple cruises along one transect the rate of increase of C_{ant} during the time interval spanning these cruises. This TSR approach is applied to a suite of 10 cruises along the Prime Meridian transect in the Southern Ocean during the 1973–2008 time interval. The inclusion of 10 cruises aims to minimize the effects of systematic errors in both the suite of ancillary measurements and in the measured C_T values. For 10 cruises, one overall MLR relationship is determined. Next, this overall relationship is used to calculate C_T^{TSR}, and by comparison with actually measured C_T, the $C_{residual}^{TSR}$ is derived. Finally $C_{residual}^{TSR}$ is regressed against sampling date (1973–2008). Following the same premises as the MLR and eMLR approaches, it is expected that increasing (over time) values of $C_{residual}^{TSR}$ reflect the increase in the concentration of C_{ant} in a water mass. As with the MLR-method, the application of the TSR approach does not require knowledge of the surface water gas disequilibria or remineralization ratios.

Seasonal variability in C_T in shallow waters is to a large extent represented by the MLR (Friis et al., 2005). Therefore, the TSR method allows the determination of time trends in C_{ant} (i.e., $C_{residual}^{TSR}$) in shallow waters. This in contrast with C_T^0 and C_T, which both are expected to show strong variations in shallow waters between the different seasons in which the data were collected.

4. Data collection

The shipboard methods of the most recent cruise are described (Section 4.1), followed by the chosen database of the preceding nine cruises (Section 4.2). Of all ten cruises, stations south of ~55°S and (generally) within 5° of longitude from the Prime Meridian were selected, representative for the Weddell Gyre. The locations of all stations are shown in Fig. 3. The cruises span the period from 1973 to 2008.

4.1. Shipboard analyses

The most recent data used in this paper, from *PFS Polarstern* cruise ANT-XXIV/3 (Cape Town—Punta Arenas, 10 February–16 April 2008; Fahrbach and de Baar, 2010) have not been published before. During this cruise, about 2800 samples were analyzed on two identical instruments (VINDTA 3C, MARIANDA, Kiel, Germany), with each instrument measuring both C_T and A_T. Collection and analysis was in accordance with the standard operating procedures outlined by Dickson et al. (2007). Samples were analyzed immediately after sampling, hence were not poisoned. Occasionally, samples were analyzed on both instruments concurrently, thereby allowing for instrument-to-instrument comparison.

Measurements of C_T were performed using the coulometric method (Johnson et al., 1993). Determinations of A_T were performed by an acid titration following the standard settings of the VINDTA (Mintrop et al., 2000). In order to set the measurement accuracy, certified reference material (CRM, Dickson, 2001) was analyzed at least three times per day. On both instruments, measurements of CRM deviated from the certified values less than 0.5% for both C_T and A_T (i.e., less than circa 12 μmol kg^{-1}). Post-cruise processing and correction of the data resulted in a dataset that is deemed to be of excellent quality for C_T, with typical short-term reproducibility of around 1.4 μmol kg^{-1} for both instruments.

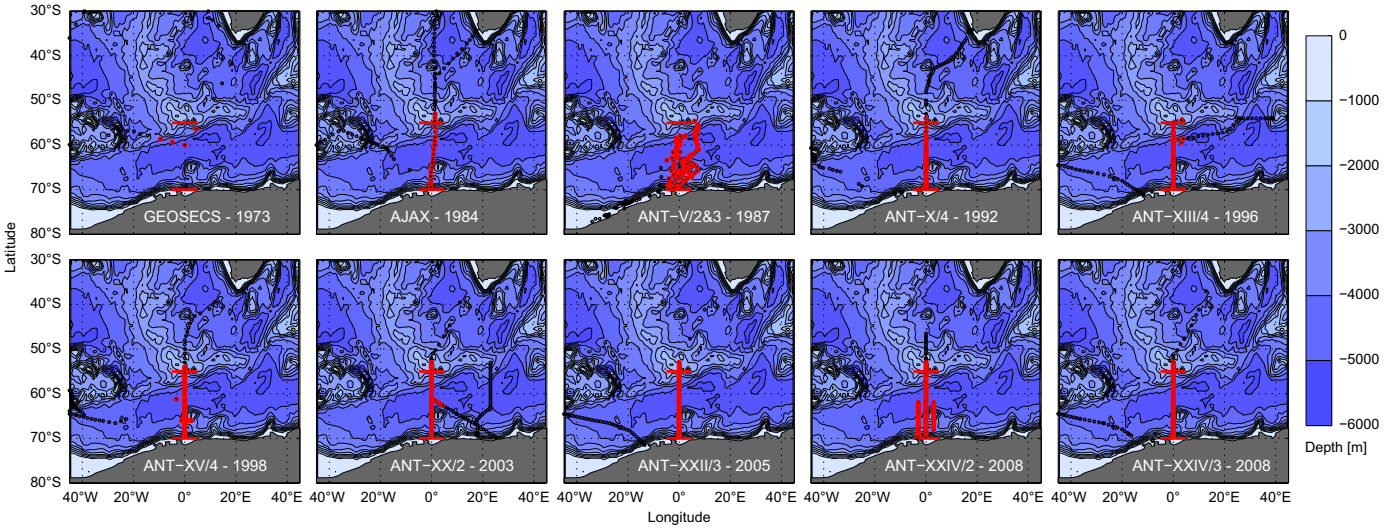

Fig. 3. Locations of the oceanographic sampling stations (red dots) of the 10 cruises used in this study. Black dots indicate locations of stations that were not used. The color scale represents the bottom topography, in 1000 m intervals. The two horizontal red lines (at 55°S and 70°S) in each panel respectively indicate the northern and southern extent of the part of the section that is investigated in this study. For several cruises, data from a few stations north of 55°S are used in the data gridding procedure.

Intercomparability of the instruments is considered to be excellent, with the difference in final C_T values between them (as inferred from about 400 samples that were run on both instruments) being 0.1 ± 1.9 μmol kg^{-1}. Results of C_T of the two instruments were merged into one dataset, of which the overall accuracy is estimated to be better than ± 2 μmol kg^{-1}. Results for A_T of one of the two instruments were discarded due to excessive drift. The estimated accuracy of the retained A_T dataset of the other instrument is ± 4.0 μmol kg^{-1}.

Data for dissolved oxygen was obtained from *in situ* sensors that were regularly calibrated against Winkler titrations, with a reported final accuracy of ± 4.5 μmol kg^{-1}. Measurements of dissolved nutrients (silicate, phosphate and nitrate) were performed colorimetrically and on board with an auto-analyzer. The combined accuracy and precision of these three measurements is considered to be better than $\pm 0.5\%$, $\pm 0.5\%$ and $\pm 1.0\%$, respectively. Measurements that were concurrently made on a preliminary batch of the novel reference material for nutrients in seawater (RMNS, distributed by KANSO co. www.kanso.co.jp; Aoyama et al., 2008) confirm this accuracy.

A more detailed account of these shipboard methods is provided in electronic Supplement S1.

4.2. Additional data

From the GLODAP 1.1 database (Key et al., 2004) and the CARINA database (Key et al., 2010) the data of six cruises in the vicinity of the 0°-meridian were extracted (Table 3). For each cruise, we used the data that had received primary quality control (outliers removed, conversion to common units), but were not yet adjusted for internal consistency, because for our application the desired internal consistency will be tailored to the local region. (Please notice that the final product of GLODAP and CARINA has been adjusted for global internal consistency). Data of C_T of cruises ANT-XV/4, ANT-XXII/3 and ANT-XXIV/2, which are not available in GLODAP or CARINA, have been described before and were obtained from the respective investigators (see references in Table 3).

5. Data processing

This study aims to quantify the rates of storage of C_{ant} in the Weddell Gyre, using data from 10 cruises conducted between 1973 and 2008. The use of multiple cruises is expected to reduce the susceptibility of the results to biases in individual cruises. Firstly, we will determine time trends directly in the actual measured data of C_T that have been collected during multiple cruises along the same ocean section. Secondly, we perform a similar time trend assessment but now using calculated C_T^0 (Section 3.1.1), relying on additional measured variables (θ, S, O_2 and A_T). Lastly, the determined time trends of C_T will be separated into their natural components and anthropogenic (i.e. C_{ant}) components using the TSR method outlined in Section 3.3. Moreover, for the sake of comparison with previous studies in

Table 2
Definition of water mass cores as used throughout this paper. 'Shallow' is obviously not a formal water mass but this layer is defined because it potentially shows most clearly the time trends in properties related to the uptake of anthropogenic CO_2 from the atmosphere. Note that the WSDW does not have a formal core since it is part of the gradient between WDW and WSBW. Of the three deeper water masses the limits of salinity and θ follow the definition by Carmack and Foster (1975), although the temperature range for WSDW has been slightly constricted in order to retain just the samples from the core (or rather 'middle layer') of the water mass. The latitudinal constraint of 58°S–63°S was added to prevent inclusion of samples (or grid points) close to the continental slope of Antarctica and to restrict the sampling to the meridional range that included data from the most cruises. Actual water masses may have a wider extent than those defined here. Note that the 'lWDW/uWSDW-normalization' performed in this study uses data of (θ: −0.4 to 0.2 (°C) and latitude: 57°S–66°S), i.e., from the deeper extent of the WDW and the upper extent of the WSDW, and from a slightly wider latitudinal range than the water masses defined in this table.

Water mass/layer	Abbreviation	Latitude (°S)	Depth (m)	Salinity	θ (°C)
(Upper 200 m)	SHALLOW	58–63	<200	–	–
Warm Deep Water	WDW		–	>34.6	>0
Weddell Sea Deep Water	WSDW		–	>34.64	-0.5 to -0.2
Weddell Sea Bottom Water	WSBW		–	>34.6	<-0.7

Table 3
Relevant details of the cruises of which data are used in this study. Date refers to the months of relevant sampling at the Prime Meridian. Adjustments applied to the data are additive in μmol kg^{-1} for C_T and A_T, and multiplicative for the other parameters (rounded to the nearest 0.5%). Adjustments without brackets are those applied in the current study, required to obtain consistency in the lWDW/uWSDW (Section 5.1). Adjustments between brackets are those suggested in the CARINA and GLODAP dataset compilation efforts, for comparison. The column 'CRM' states the use of Certified Reference Material (CRM; Dickson, 2001) during the analyses of C_T and A_T. In the most recent cruise ANT-XXIV/3 (2008) reference material (Aoyama et al., 2008) was additionally used in nutrient analyses. For background information regarding these cruises please refer to the listed references or the CARINA (http://cdiac.ornl.gov/oceans/CARINA/) or GLODAP (http://cdiac.ornl.gov/oceans/GLODAP/) literature.

Cruise	Date	Ship	Adjusments performed to the data						C_T-relevant reference	CRM
			C_T	A_T	O_2	NO_3	PO_4	Si		
GEOSECS	Jan 1973	Knorr	−0.6[a] (0)	−5 (−10)	0% (−1%)	+1% (0%)	+1% (+2%)	−2% (0%)	Bainbridge (1981)	No
AJAX	Jan–Feb 1984	Knorr	+10.9 (+8)	+8 (0)	−2% (−1%)	−1% (0%)	+2% (0%)	−1% (−2%)	Chipman et al. (1986)	No
ANT-V/2–3	Jul–Dec 1986	Polarstern	+12.8 (+12)	+7[b] (0)	0% (0%)	+3% (+3%)	+0.5% (0%)	−0.5% (0%)	Schnack-Schiel (1987)	No
ANT-X/4	Jun–Jul 1992	Polarstern	+2.1 (0)	No data	−1% (0%)	−0.5% (−2%)	−0.5% (−2%)	0% (−2%)	Hoppema et al. (1995)	No
ANT-XIII/4	April 1996	Polarstern	−0.6 (−4)	No data	−0.5% (+1%)	+3.5% (+2%)	+2.0% (1%)	+2.0% (+5%)	Hoppema et al. (1998)	Yes
ANT-XV/4	May 1998	Polarstern	−1.8 (NA)	No data	−0.5 (NA)	−1.0% (0%)	−2.0% (0%)	−0.5% (NA)	Hoppema (2004)	Yes
ANT-XX/2	Dec 2002	Polarstern	+2.0 (NA)	No data	+0.5% (NA)	−2.0% (NA)	No data	−2.0% (NA)	Bakker et al. (2008) and Geibert et al. (2010)	Yes
ANT-XXII/3	Feb 2005	Polarstern	−0.6 (NA)	No data	+2.5% (NA)	−1.5% (NA)	0% (NA)	0% (NA)	Hoppema et al. (2007)	Yes
ANT-XXIV/2	Jan 2008	Polarstern	+0.6 (NA)	0 (NA)	0% (NA)	0 (NA)	No data	No data	Hauck et al. (2010)	Yes
ANT-XXIV/3	Feb 2008	Polarstern	+0.3 (NA)	−1 (NA)	+1.5% (NA)	0% (NA)	0% (NA)	0% (NA)	This work	Yes

[a] C_T of GEOSECS was measured potentiometrically, for all other cruises C_T was measured coulometrically.
[b] A_T of ANT-V/2&3 was calculated by GLODAP from C_T and pCO_2.

the region, the concentration of C_{ant} will be determined with another approach, the TrOCA method.

5.1. Normalization in lower Warm Deep Water (WDW) and upper Weddell Sea Deep Water (WSDW)

In the Weddell Gyre, the southernmost part of the 0°-meridian section, the lower extent of the WDW together with the upper part of the WSDW, is considered the least ventilated water body (Fahrbach et al., 2011; Behrendt et al., 2011; to be concise, this combined water body will in the context of the normalization procedure be referred to as lWDW/uWSDW). Indeed, over the 1973–2008 period of observations, the C_T in this water body is in steady state (Fig. 4), except for the strongly outlying data of AJAX (1984) and ANT-V/2&3 (1986). Moreover, the observed values of major nutrients (silicate, nitrate and phosphate) and dissolved oxygen in the lWDW/uWSDW also are in steady state, i.e., there are no systematic changes discernable in biogeochemical processes (data not shown). Nevertheless, for each cruise there may exist a systematic offset due to calibration uncertainties. In order to remove these offsets (that in turn might give rise to erratic time trends), a normalization is applied to bring the values in the WDW of each cruise to the mean of all 10 cruises. Following Hoppema et al. (2001), for each cruise a subset of the data (latitude: 57°S–66°S, potential temperature (θ): −0.4 °C to 0.2 °C) of the parameter to be adjusted is linearly regressed against θ and the intercept at θ=0 °C is determined. For each cruise, the difference between this intercept and the mean intercept at 0 °C of the entire dataset (in the case of C_T: 2262.7 μmol kg^{-1}, see Fig. 4) is taken as the required adjustment. Adjustments determined in this manner for all relevant parameters of all cruises are listed in Table 3 (i.e., C_T, A_T, O_2, NO_3, PO_4, Si. Data of CFCs were not adjusted). At the latitudinal range considered, the used temperature range coincides with a depth range of about 800–2200 m, i.e., the lWDW/uWSDW. The NADW in the South Atlantic Ocean is much larger and even less ventilated than the lWDW/uWSDW and is deemed an even more suitable reference water mass, but cannot serve that purpose because five of the ten cruises in this study did not sample the NADW.

The spread of measurements around the regression line (Table 4, column 'rmse') is illustrative of the precision of the data of each cruise. Clearly, the precision of the analysis of C_T has generally improved over time, from 4.0 μmol kg^{-1} during GEOSECS in 1973 to 1.3 μmol kg^{-1} or 2.2 μmol kg^{-1} for ANT-XXIV/2 and ANT-XXIV/3, respectively. The thus adjusted datasets for C_T

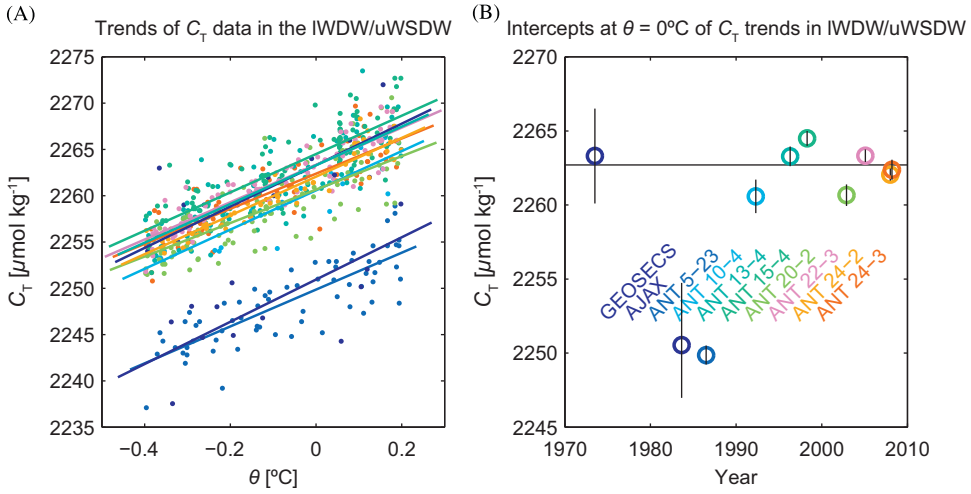

Fig. 4. Example for C_T of the procedure followed to normalize cruise data in the lower WDW and upper WSDW (lWDW/uWSDW). See Section 5.1 for details. (A) Regressions of measured C_T(μmol kg^{-1}) versus potential temperature (θ) (°C) of all 10 cruises. The strongly outlying regression lines represent the data of cruises AJAX (1984) and ANT-V/2&3 (1987). (B) The determined intercepts at θ=0 °C of the regressions in panel (A). The black horizontal line indicates the mean intercept (2262.7 μmol kg^{-1}) of all cruise data (ANT-V/2&3 excepted). The black vertical lines represent the 95% confidence interval of each intercept. Data of each cruise were adjusted to make the cruise-specific intercept coincide with the mean intercept of all (non-outlying) cruises.

Table 4
Details of the regression of C_T versus potential temperature of cruise data from the deeper part of the WDW and the upper part of the WSDW (lWDW/uWSDW). rmse: root mean square error (i.e., measure of spread of data around the regression line). Data were adjusted to yield an intercept of 2262.7 μmol kg^{-1}. Although not obvious from these results, the data of C_T of AJAX (1984) were deemed to be of insufficient quality for inclusion in this study. Southerly, deep data of ANT-X/4 are deemed to be erroneously high, and are also not further used in this study either (see also Fig. 5). See text Section 5.1 for details.

Cruise	intercept	Slope (°C^{-1})	rmse (μmol kg^{-1})	*n*	Adjustment (μmol kg^{-1})	Discarded data
GEOSECS	2263.3 ± 3.2	22.4 ± 13.5	4.0	15	−0.6	None
AJAX	2250.8 ± 2.1	21.2 ± 9.9	3.9	23	+10.9	All data
ANT-V/2&3	2249.2 ± 0.9	18.7 ± 4.4	2.7	48	+12.8	None
ANT-X/4	2260.5 ± 1.0	21.0 ± 5.1	2.1	22	+2.1	< 63°S and < 1500 m
ANT-XIII/4	2263.3 ± 0.6	20.9 ± 2.9	2.4	91	−0.6	None
ANT-XV/4	2264.5 ± 0.5	20.7 ± 2.6	2.4	105	−1.8	None
ANT-XX/2	2260.8 ± 0.7	18.7 ± 3.3	3.3	116	+2.0	None
ANT-XXII/3	2264.3 ± 0.4	20.2 ± 2.1	1.7	79	-0.6	None
ANT-XXIV/2	2262.0 ± 0.4	20.9 ± 2.0	1.3	54	+0.6	None
ANT-XXIV/3	2262.4 ± 0.7	18.9 ± 3.1	2.2	64	+0.3	None

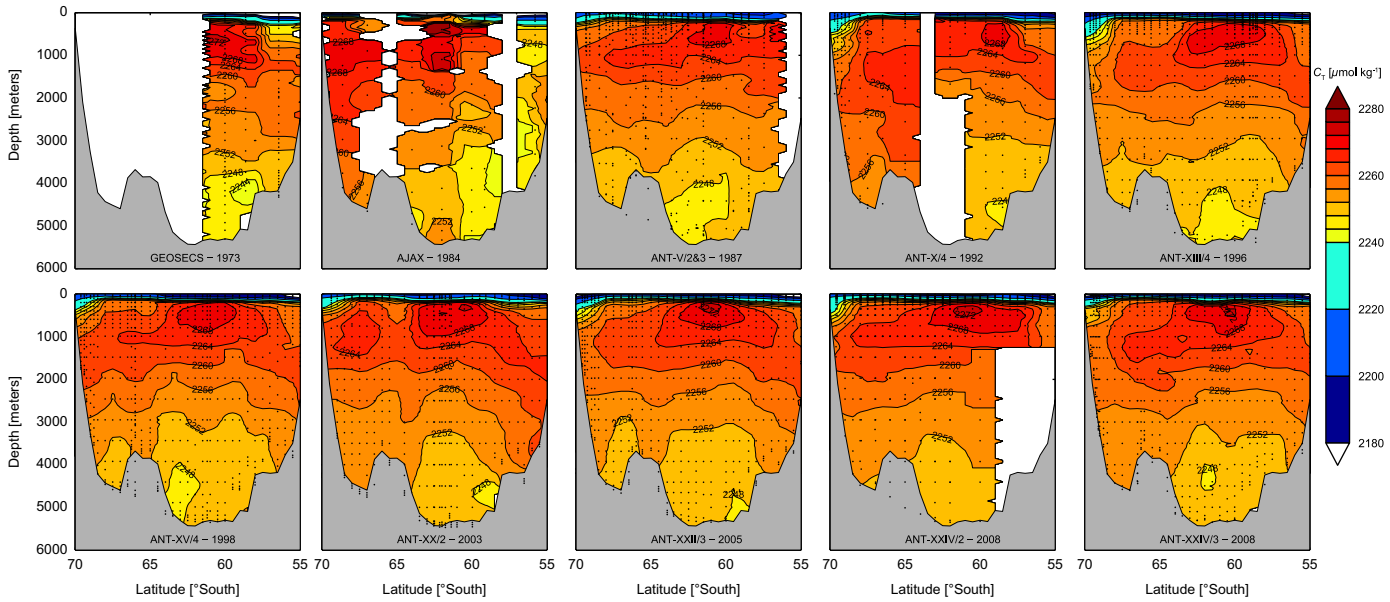

Fig. 5. Section plots for the 10 cruises used in this study of C_T (after normalization in the lWDW/uWSDW; see text Section 5.1 for details). Note that southerly, deep data ($>63°S$, >1500 m) for ANT-X/4 and all data of AJAX are shown in this figure, although these data are not further considered in this study.

and other parameters are highly internally consistent within the lWDW/uWSDW. However, the C_T data of AJAX (1984) are deemed to be of insufficient quality for this study due to low spatial sampling resolution and significant station-to-station biases that cannot be objectively resolved. Therefore, the C_T data of AJAX are excluded from further analysis (the remaining data of CFCs and A_T of AJAX will be used). Similarly, the southerly deep data (south of 63°S and deeper than 1500 m) of cruise ANT-X/4 are considered erroneously high by up to 7 μmol kg^{-1} and are also excluded from analysis. Fig. 5 shows sections of the lWDW/uWSDW-normalized C_T data. Although they are not (all) used in further analyses, the data of AJAX and ANT-X/4 are shown in Fig. 5 for completeness. The performed adjustments are of similar magnitude as those applied in CARINA and GLODAP (Table 3).

5.2. Data gridding

Toward discerning a time trend over 35 yr, all cruises are assigned equal weight. If this is not done, then a straightforward regression would cause overrepresentation of those cruises that have most measurements. Equal weighting of the data of each cruise is accomplished by resampling all data of interest (S, θ, CFC-12, C_T, A_T, O_2, nutrients) onto a common grid (spacing: 100 m depth and 0.5° latitude). The longitude of all data is set to 0°E. Bottom topography is assumed to be the same for all cruises, as extracted from a bathymetric dataset of the mean topography between 2°W and 2°E. Care was taken not to allow the gridding routine to extrapolate data too far into depths or latitudes where infact no samples were collected.

5.3. Consideration of oxygen

Some cruises retain significant localized bias for O_2, even after the lWDW/uWSDW-normalization procedure outlined above. In order to illustrate this, we obtain a 'best' or 'mean' section of O_2 by averaging the very consistent O_2 sections of recent cruises ANT-XIII/4, ANT-XV/4, ANT-XX/2 and ANT-XXIV/2, and make section plots of the difference of this O_2^{mean} and each of the O_2 datasets of all ten cruises used in this study (Fig. 6). It may be observed that the applied single-adjustment approach is not sufficient for eliminating all biases in the O_2 datasets of all cruises. For example, an offset may be seen for ANT-XXIV/3 in the deep water between 60°S and 65°S. This anomaly is not observed for ANT-XXIV/2 only 2 months earlier. Similarly, cruises GEOSECS, ANT-V/2&3 and ANT-XXII/3 also appear to have calibration problems, although for GEOSECS, which is far in the past from the subsequent cruises, deviations in the deep water arguably might be reflective of genuine changes in the deep Weddell Sea. Based on these observations, this study ignored the O_2 data of ANT-XXII/3 and ANT-XIV/3, and of selected stations of ANT-V/2&3 (north of 63°S) and GEOSECS (north of 57°S). The magnitude of these (local) offsets (about 2–5 μmol kg^{-1}) is about as large as the stated overall accuracy of O_2 of cruise ANT-XXIV/3 (± 4.5 μmol kg^{-1}, see Supplementary material), and much larger than the $\pm 1\%$ (locally about ± 2–3 μmol kg^{-1}) that is often stated for the accuracy of oxygen measurements in general. The uncertainty about the accuracy of O_2 measurements (in this study and in general) may jeopardize the application and interpretation of the back-calculation techniques that require O_2 (C_T^0, TrOCA). In the back-calculation concept, an erroneously low O_2 yields a C_T^0 that is also too low, because a too large fraction of the measured C_T is considered to result from remineralization of organic matter (see Eq. (1)).

5.4. Derivation of necessary variables

The following variables were derived from the gridded original data.

$\mathbf{C_T^0}$: Values of preformed C_T (i.e., C_T^0) were calculated for each grid point of each cruise using Eq. (1) (Section 3.1.1). The required values of A_T^0 and O_2^{sat} were obtained using the parameterizations of Sabine et al. (1999) and of Weiss (1970), respectively. Because the present study concerns the increase in C_T^0 over a certain period rather than its exact value, the determination of the pO_2 disequilibrium is not required, and we assume $\Delta pO_2 = 0\%$. The values of the ratios $\psi_{O:C}$ and $\psi_{O:N}$ are taken from Anderson and Sarmiento (1994) as 117/170 and 16/170, respectively.

$\mathbf{A_T^{MLR}}$: Measurements of A_T are available from 4 of the 10 cruises. To improve the availability of A_T (a requirement for the application of the C_T^0 and TrOCA methods), an MLR was performed of the available (WDW-adjusted) data of A_T versus [salinity, θ, silicate, depth, latitude]. With the derived coefficients, an artificial

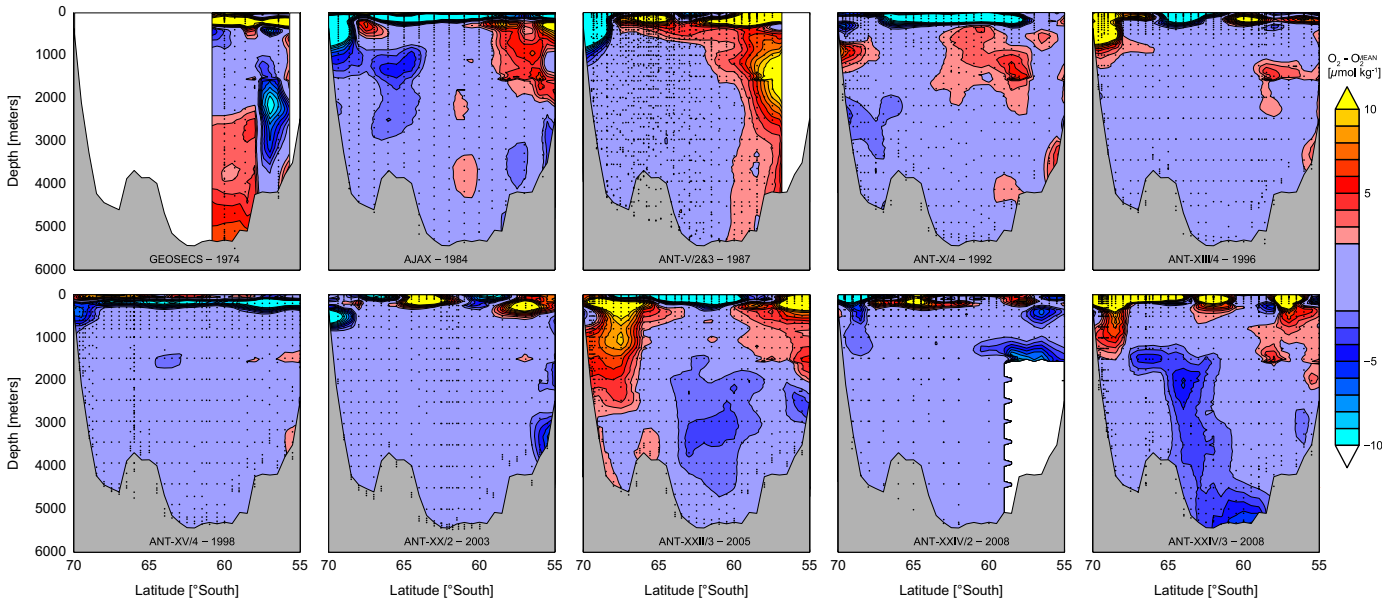

Fig. 6. Section plots for the 10 cruises used in this study of the difference between (lWDW/uWSDW-normalized) O_2 and O_2^{mean}. The latter is defined as the mean lWDW/uWSDW-normalized O_2 of four selected, mutually consistent cruises: ANT-XIII/4, ANT-XV/4, ANT-XX/2 and ANT-XXIV/2. These section plots are deemed to be indicative of station-to-station bias in the reported data of O_2. These biases are not accounted for by the single normalization performed in this study. Because the data of O_2 of ANT-XXIV/3, ANT-XXII/3 and of selected stations of ANT-V/2&3 (north of 63°S) and GEOSECS (north of 57°S) exhibit such bias they are excluded from this study, but are retained in this figure.

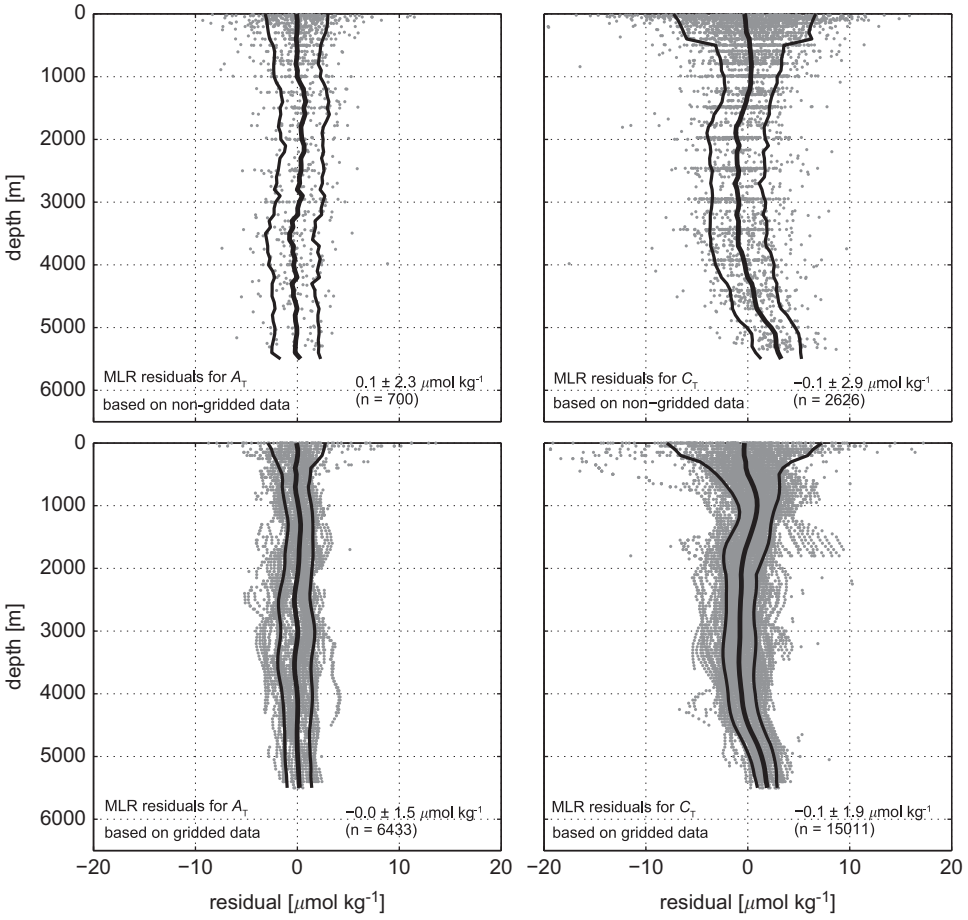

Fig. 7. Depth profiles of the residuals of multivariate linear regressions (see Section 5.4) of data of (left column) A_T versus [salinity, θ, silicate, depth, latitude] and (right column) C_T versus [salinity, θ, silicate, phosphate, depth]. The top row comprises non-gridded data, bottom row comprises gridded data. Thick lines indicate the mean and standard deviation of the residuals over a moving 500 m interval. The overall standard deviation of each profile is provided as text in each panel.

variable A_T^{MLR} was generated. In order to optimally represent the measured values of A_T over the entire section, separate MLRs were performed for each of four intervals of potential density. The procedure was performed both for non-gridded and gridded data, in order to verify the robustness of the gridding routine. The resulting residuals of the regressions are presented in Fig. 7 (panels A, C). It can be observed that the residuals are small and neutrally distributed around zero (0.1 ± 2.3 and 0.0 ± 1.5 μmol kg^{-1} for non-gridded and gridded data, respectively). The shapes of the profiles are highly comparable, confirming the suitability of the employed gridding method. Since the predictive parameters were measured more often than A_T itself, values of A_T^{MLR} could be obtained for 9 of the 10 cruises (no silicate data of cruise ANT-XXIV/2 are available). At any location, the values of derived variable A_T^{MLR} are much more homogenous between the cruises than the original A_T values, which are not further used in this study. It must be noted that this application of an MLR removes any conceivable time trend from the A_T data if this trend is not reflected in any of the constituent parameters of A_T^{MLR}. This is in accordance with the common assumption that, as yet, there has been no anthropogenic influence on A_T distributions since the onset of the industrial revolution.

C_T^{TSR} and $C_{residual}^{TSR}$: As part of the TSR approach (Section 3.3), we performed an MLR between the measurements of C_T and ancillary variables [salinity, θ, depth, A_T^{MLR}, phosphate, silicate], both for the gridded dataset and for the non-gridded dataset. All relevant data from all cruises in this study (i.e., the full 1973–2008 era) were used in a single MLR. As outlined in Section 5.3, we suspect the presence of significant inaccuracies in some of the measurements of O_2. To avoid complicating the attribution of resulting time trends in $C_{residual}^{TSR}$, the MLR did not use O_2 as an estimate of remineralization but relied solely on phosphate and silicate for this purpose. This is akin to the approach of Friis et al. (2005), who opted for the use of a nutrient (phosphate) instead of O_2-based AOU, because use of the latter resulted in a non-normal and depth-varying distribution of residuals. The residuals of the regression (Fig. 7, panels B, D) are reasonably small (-0.1 ± 2.9 and -0.1 ± 1.9 μmol kg^{-1} for non-gridded and gridded data respectively) and provide confidence that a suitable selection of independent parameters was chosen. The slanted shape of the residuals profile does not jeopardize our application, since we are solely interested in the *time trends* of the residuals, rather than their actual values.

5.5. Determination of time trends along the section

For each of the measurements (and derived variables) of interest, time trends were determined at each of the grid points as follows: of each of the cruises, the value of the grid point of interest and those of the grid points immediately surrounding it, were extracted. These values (up to 90 for each grid point: there are up to 10 cruises present at each grid point, and each grid point is surrounded by up to 8 other grid points) were regressed against their time of sampling, using an ordinary least squares linear fitting routine. All grid points weighted equally in the regression. This procedure makes the results slightly less sensitive to an occasional outlying value in the grids. Since no resolvable gradients are expected on the short spatial scale from one grid point to another, this step does not sacrifice spatial resolution. The results of the regression at each grid point allow for

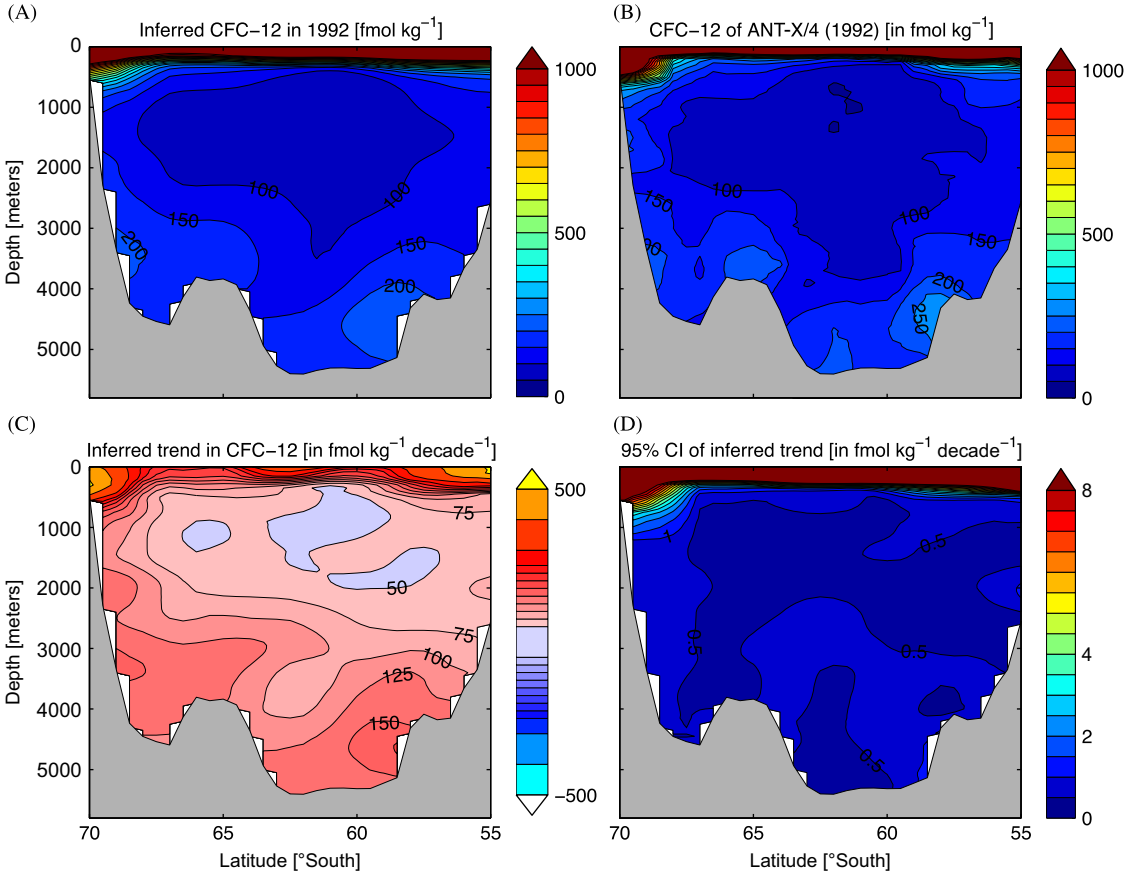

Fig. 8. Example of results of the determination of linear trends in CFC-12, using all available data (i.e., from 1984 to 2005). (A) inferred CFC-12 section in 1992; (B) actual section from 1992, measured during cruise ANT-X/4; (C) determined linear time trends of CFC-12 over the 35 year period; (D) standard error of the time trend estimates of panel 8C. Trends with high relative standard errors are generally located in shallow waters. This is where the diminishing atmospheric increase is most closely tracked and, additionally, where temperature-driven seasonal oscillation of the concentrations of CFC-12 may further invalidate the assumption of linearity of time trends.

the derivation of parameter values for those years where data is not available. In general, trends derived in this way in the upper ~400 m of the Weddell Gyre should not be taken to be representative of the underlying data, due to seasonality in the upper shallow waters and the limited resolution of used grid relative to the vertical variability of the water column at these depths. However, trends in $C^{TSR}_{residual}$ do allow for interpretation in the shallow water column (Section 3.3).

To illustrate this approach of linear fitting through gridded data, we process data of CFC-12. Fig. 8 shows the concentrations of CFC-12 in 1992 as inferred from the time trends through the measurements obtained on the 7 coverings of the section (AJAX, 1984 to ANT-XXII/3, 2005). Also shown are actual measurements in 1992 (ANT-X/4), as well as the inferred time trends and the uncertainty associated with these time trends. The inferred concentrations in 1992 compare very well with the gridded data of ANT-X/4 (slope of regression of data below 1000 m depth: 0.98 ± 0.02, $r^2 = 0.87$, $p < 0.001$).

Even though the results obtained from CFC-12 serve an illustrative purpose only, we note that the use of linear regressions for CFC-12 does not do justice to the well known, distinctly non-linear concentration history of this compound in the atmosphere and the surface ocean. However, the stabilization and decrease of the atmospheric concentration of CFC-12 since approximately 2003 has not likely penetrated into the deep Weddell Sea yet (Klatt et al., 2002; Huhn et al., 2008). Therefore, an approximately linear rise in interior ocean concentrations may still be expected, and is indeed observed (Fig. 9, see text Section 5.6 for details).

5.6. Determination of time trends in water mass cores

The determination of time trends at fixed locations (latitude, depth) as outlined in Section 5.5, yields results that may be plotted to reveal the spatial pattern of such trends (for example, Fig. 8C). However, the results of that procedure may occasionally be ambiguous not only because of the sometimes small amount of samples represented by each grid point, but also because of hydrographical variability at each grid point. For example, the location of a particular water mass may vary somewhat through time and is thus not always present at the same location on the grid. Detection and quantification of time trends at such a location may therefore be jeopardized. To ensure that time trends within the proper cores of water masses are nonetheless optimally quantified, an additional analysis of the data was performed in which all grid points that belonged to the core of a particular water mass (as determined by their S and θ properties, see Table 2) were pooled, and time trends were determined for the data in each of these data pools. This procedure was performed for both the gridded and the non-gridded data, again in order to be able to verify that no inaccuracies result from the gridding routine. The time trends were determined by calculating for each cruise the mean values of the data in the water mass cores. Subsequently, an ordinary least squares linear fit against time was determined through these averages.

A sensitivity analysis was performed using a simple statistical model. We assume that the remaining inaccuracy (after the lWDW/uWSDW-adjustment) of the measurements of C_T performed before the introduction of CRM (i.e., the cruises in the period 1973–1992) is smaller than 4 μmol kg^{-1}. The subsequent 6 cruises did use CRM and are assumed to be accurate to within 2 μmol kg^{-1}. Under those assumptions, and taking into account the analytical noise in the measured C_T data (Section 5.1), trends smaller than circa 1 μmol kg^{-1} decade^{-1} fall within the statistical uncertainty of the method (at the $p < 0.05$ level).

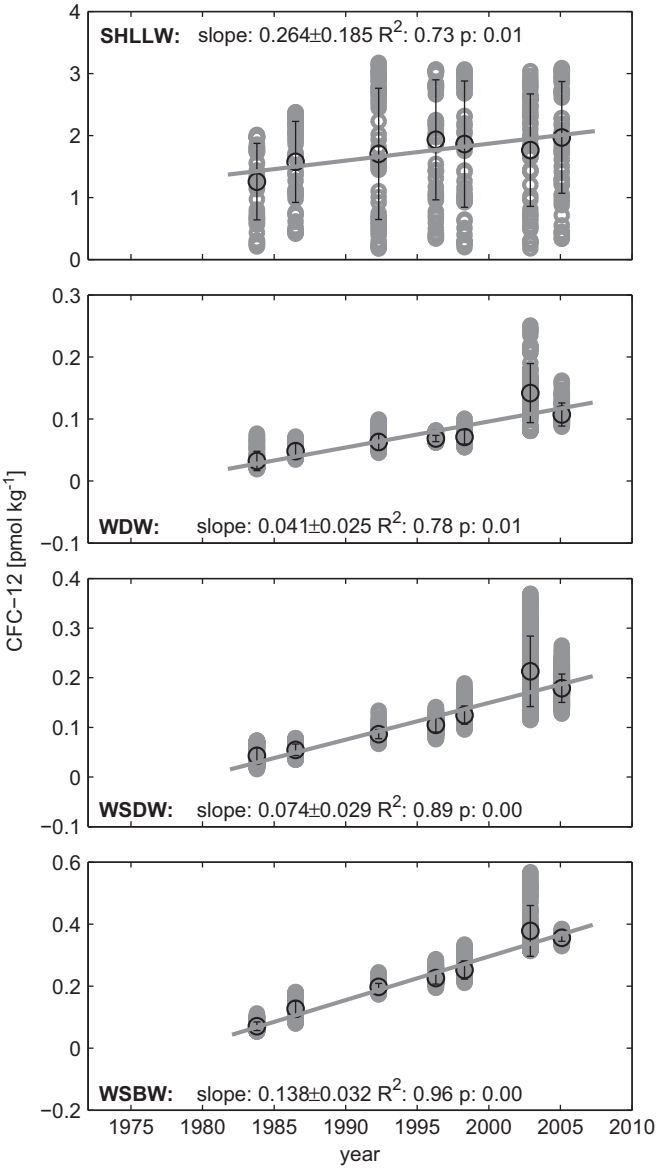

Fig. 9. Time trends in the gridded data of CFC-12 (pmol kg^{-1} decade^{-1}) in the upper shallow waters and in the cores of three water masses (WDW, WSDW, WSBW; see Table 2), determined using ordinary least squares regression. See text Section 5.6 for details.

5.7. Determination of C^{TrOCA}_{ant} for 2005

For the sake of comparison with the findings of previous studies, the concentration of C_{ant} along the section is determined for the nominal year 2005 using the TrOCA method (Section 3.1.3). The required values of O_2, C_T and A_T (or rather A^{MLR}_T; Section 5.4) are obtained by taking the mean values of all cruises in the time interval from 2002 to 2008. We use the same θ-based TrOCA^0-parameterization as used by Lo Monaco et al. (2005b), which is only a slight adaptation of the parameterization originally provided by Touratier and Goyet (2004b).

5.8. The carbonate system of the Weddell Gyre in a high-CO_2 world

The continued uptake by the oceans of anthropogenic CO_2 from the atmosphere will cause shifts in the oceanic carbonate system. Most notably, a strong reduction is predicted of the concentrations of carbonate ion [CO_3^{2-}] and hydroxide ion [OH^-]. These changes are of major importance for the solubility of (biogenic) $CaCO_3$ (Feely et al.,

2004; Orr et al., 2005) and for the speciation of trace metals (Millero et al., 2009). In order to briefly investigate the presence of these effects in the Weddell Gyre, values were calculated of [CO_3^{2-}], pH (representing the decreasing [OH^-]), and of the saturation states of the $CaCO_3$-structures aragonite and calcite (Ω_{AR} and Ω_{CA}) from the gridded data of [S, T, C_T, A_T^{MLR}, phosphate and silicate] using CO2SYS for MATLAB (van Heuven et al., 2009). Trends were determined in these data as in Section 5.6.

6. Results

6.1. Spatial distribution of time trends along the section

CFC-12: The pattern of trends found in CFC-12 (Fig. 8C) in the deep waters reflects current knowledge about the ventilation processes of the Southern Ocean (e.g., Klatt et al., 2002). The strongest sub-surface increases are visible in the WSBW, flowing eastward along the southern side of the Mid-Atlantic Ridge (MAR), and along the Antarctic continental slope in the westward flowing water that makes up the southern limb of the Weddell Gyre. The core of the WDW (at 500–1500 m, 57–63°S) shows a very low rate of increase in CFC-12. Because the CFC-12 concentrations at the surface of the water column tightly track the (distinctly non-linear) atmospheric CFC-12 concentration history, the method of linear fitting is not applicable at these shallower depths, as is also evidenced by the high uncertainties associated with the trends (Fig. 8D). Therefore, results obtained in the upper 400 m will not be discussed and should not be taken to accurately reflect the rates of accumulation of CFC-12. In deeper waters, this problem is likely not yet as prominent (see Section 5.1). A detailed look at the trends in the cores of the water masses (Fig. 9, Table 5) shows the CFC-12 to still increase approximately linearly.

C_T: The spatial distribution of determined time trends in C_T (Fig. 10A) qualitatively resembles that of CFC-12 in the deep region of the Weddell Gyre (Fig. 8C). Notably in the WSBW and the deeper ranges of the WSDW, rates of increase of C_T are between 0.5 and 1.75 μmol kg^{-1} $decade^{-1}$. A spatial distinction is observed between the cores of the increases in the southern and northern limb of the Weddell Gyre, in agreement with the pattern of trends in CFC-12. Again, we consider trends in C_T that were determined in the upper 400 m of the water column not to accurately reflect real trends. It is interesting to note, though, that a near-zero (or even negative) rate of increase, associated with the upwelling region south of ~60°S, prominently appears, as does an area of strong uptake (rates over 5 μmol kg^{-1} $decade^{-1}$) to the north of this divergence zone.

The near-zero rate of increase of C_T within the WDW has been dictated by the method. The inherent assumption of a constant C_T in the WDW is largely corroborated by the time trends in CFC-12, which are very small there (only about 30% of the bottom water trends). Additionally, we note again that pre-correction values of C_T in the WDW did not exhibit a trend, and that the applied corrections are small. The positive trend in C_T is also visible along the Antarctic continental slope from circa 1000 m downward, and tentatively also around 57°S, as a protrusion from the surface downward to circa 2000 m depth. These columnar features at the southern and northern limits of the Weddell Gyre resemble the observed spatial distribution of CFC-12 and the trends therein (Fig. 8A, B and C). Discussing data of CFC-11, the northern structure is interpreted by Klatt et al. (2002) as resulting from vertical mixing at the interface between the ACC and the Weddell Gyre, while the southern feature reflects the inflow from east of the Weddell Gyre of recently ventilated water.

By simple linear regression of the time trends in C_T versus those in CFC-12 for all grid points below 750 m and between 57°S and 68°S we find a significant correlation (Fig. 11):

$$dC_T/dt = 8.4 \pm 0.4 \times d\mathrm{CFC12}/dt - 0.23 \pm 0.04 \quad (n = 1875,\ R^2 = 0.48,\ p < 0.001) \tag{8}$$

The above relationship between the increases of CFC-12 and C_T is not highly significant. A better correlation than this is not likely to be expected, in part due to different equilibration times of the gases in the region of water mass formation, measurement inaccuracies and the distinctly different atmospheric histories of these gases (for a detailed treatment of the latter factor, see Tanhua et al., 2006). However, the relationship provides evidence that the observed distribution of time trends in C_T is consistent with the much more clearly resolved accumulation of CFC-12 in the deep Weddell Sea.

C_T^0: The spatial distribution of time trends in the derived concentrations of C_T^0 along our section (see Fig. 10B) is not at all in agreement with the time trends found directly in the originally measured C_T (Fig. 10A). Strongly positive trends in C_T^0 can be seen from the Antarctic continental slope northward to 62°S, whereas the WSWB shows near-zero or negative trends. The observed pattern of time trends in C_T^0 does not conform to known hydrographic pathways as exemplified by CFC-12 (Fig. 8C), suggesting that the observed time trends in C_T^0 are likely spurious. The erratic pattern of trends in C_T^0 is found to be mainly attributable to localized biases in data of O_2 (Section 5.3), which results in a reduced ability to determine time trends through use of this parameter. This sensitivity of the C_T^0 approach (and likely other approaches that use O_2) to biases of measurements of O_2 illustrates the need for future more accurate determinations of the dissolved O_2.

TSR: The spatial distribution of time trends of C_T^{TSR} (Fig. 10C; representing natural variability) are close to zero everywhere in the deep Weddell Sea except for in the WSBW, where a moderate increase is observed. The latter would suggest that part of the

Table 5
The time trends in C_T (derived in both the non-gridded and the gridded data) and in C_T^{TSR}, $C_{residual}^{TSR}$ and CFC-12 as determined within the cores of each of the four water masses SHALLOW, WDW, WSDW and WSBW. Definitions of the water mass cores are given in Table 2. Significant time trends are in bold print. Time trends in the shallow waters that are expected to be susceptible to the influence of seasonality at the surface are shown in brackets. As opposed to the underlying data of the other results in this table, the CFC data were not normalized in the lWDW/uWSDW and indicate that the core of the WDW is not entirely unventilated. Rather, it shows a rate of increase of about 30% of that of the WSBW. Although this suggests that an upward correction may conceivably have to be applied to the C_T-based results, we opt not to perform this adjustment. See text Section 7.2.

Water mass	C_T μmol kg^{-1} $decade^{-1}$ *Non-gridded data*	C_T μmol kg^{-1} $decade^{-1}$ *Gridded data*	C_T^{TSR} μmol kg^{-1} $decade^{-1}$ *Gridded data*	$C_{residual}^{TSR}$ μmol kg^{-1} $decade^{-1}$ *Gridded data*	CFC-12 pmol kg^{-1} $decade^{-1}$ *Gridded data*
SHALLOW	(+1.846 ± 3.693)	(+2.979 ± 3.181)	**(+3.878 ± 3.656)**	+0.332 ± 1.797	**(0.264 ± 0.185)**
WDW	+0.086 ± 0.298	−0.213 ± 0.720	+0.340 ± 0.362	−0.436 ± 0.520	**0.041 ± 0.025**
WSDW	+0.241 ± 0.318	+0.176 ± 0.321	+0.268 ± 0.613	−0.363 ± 0.636	**0.074 ± 0.029**
WSBW	**+1.250 ± 0.563**	**+1.151 ± 0.563**	+0.512 ± 0.832	**+0.445 ± 0.405**	**0.138 ± 0.032**

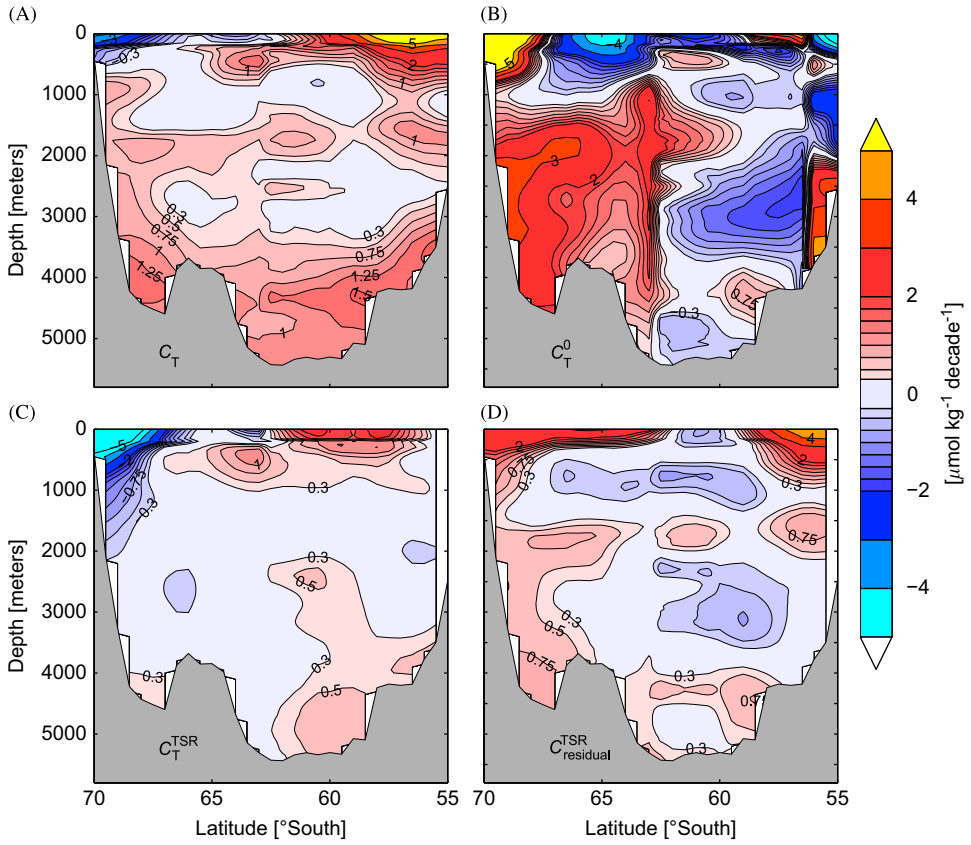

Fig. 10. Section plots of the linear time trends (μmol kg^{-1} decade^{-1}) determined through the gridded data of (A) measured C_T; (B) C_T^0, the values of back-calculated preformed C_T, which are assumed to reflect a time trend in C_{ant}, due to compensation for variable biogechemical modification of C_T; (C) C_T^{TSR}, the values of C_T predicted using a multivariate linear regression of C_T versus a suite of independent parameters, deemed to represent the component of the trends in C_T that are attributable to natural variability; (D) $C_{residual}^{TSR}$, the residuals of the TSR method, the trends in which are expected to reflect the component of the variability of C_T that is due to uptake of C_{ant} at the ocean surface. All results are based on data that were adjusted for consistency in lWDW/uWSDW. See Sections 5.5 and 6.1 for details.

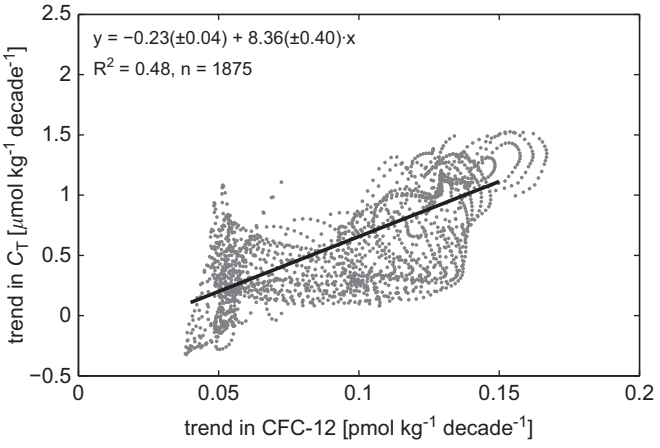

Fig. 11. Regression between the time trends determined in C_T (μmol kg^{-1} decade^{-1}) and in CFC-12 (pmol kg^{-1} decade^{-1}) at the 1875 grid points deeper than 750 m and between 68°S and 57°S. Although the non-identical atmospheric concentration histories of C_{ant} and CFC-12 formally would invalidate the use of a linear regression as performed here, the agreement is quite apparent (R^2=0.48) and provides confidence that the spatial distribution of the rates of increase of C_T is indeed related to spatial distribution of the accumulation of CFCs in the deep Weddell Gyre.

time trend in measured C_T (Fig. 10A) in the WSBW may be attributed to variability in hydrographical or biogeochemical processes in the ocean interior. Indeed, the time trend in $C_{residual}^{TSR}$ (Fig. 10D; representing the anthropogenic influence) in the WSBW is clearly smaller than the time trend in measured C_T (Fig. 10A). This is further quantified in below Section 6.2. However, away from the core of the WSBW, several features of the distribution of the time trends in measured C_T are reflected in the distribution of time trends in $C_{residual}^{TSR}$. Most notably, the columnar feature adjacent to the Antarctic continental slope (see also Section 6.1) and the southernmost deepest core (66°S–69°S, >3500 m) are observed (although their magnitude is slightly smaller than the time trends observed directly in measured C_T, Fig. 10A). Additionally, in both C_T and $C_{residual}^{TSR}$, a strong time trend is seen in the upper waters (<500 m) north of the diversion zone at 60°S. These results indicate that at these locations, a significant fraction of the time trends observed in measured C_T may be attributed to uptake of C_{ant} at the surface of the Weddell Sea.

Lastly, a striking difference between time trends in C_T and $C_{residual}^{TSR}$ is noted that, as we will argue, may be explained by the fact that values of (and time trends determined in) $C_{residual}^{TSR}$ are insensitive to seasonality. Namely, in the upper waters near the Antarctic continent (south of 66°S and shallower than 500 m), the $C_{residual}^{TSR}$ shows a marked increase with time (about 2–3 μmol kg^{-1} decade^{-1}; Fig. 10D) indicating that the anthropogenic component of C_T is increasing there. This increase is not evident from in C_T or C_T^{TSR}, which both show a negative time trend (Fig. 10A and C). Both these latter two inferred decreases are conceivably strongly influenced by the combination of strong seasonal variability in these upper waters and the unbalanced seasonal distribution of the cruises, and are indeed statistically not significant (data not shown). Because the natural seasonal variability in C_T over the 1973–2008 era is by the TSR method related to independent parameters (mainly temperature), this variability is nicely replicated in the values of C_T^{TSR}. However, the

gradually increasing C_{ant} in these waters is not expressible in terms of an independent variable, and is therefore visible as a time trend in $C^{TSR}_{residual}$.

6.2. Time trends determined in water mass cores.

Fig. 12 and Table 5 present the determined time trends in the four water masses defined in Table 2 (SHALLOW, WDW, WSDW, WSBW). On the one hand the time trends of C_T in the WSDW are quite small and non-significant at $+0.241 \pm 0.318$ and $+0.176 \pm 0.321$ μmol kg^{-1} decade^{-1} for the gridded and non-gridded data, respectively. On the other hand, the time trends of C_T in the WSBW are sizable and significant at $+1.151 \pm 0.563$ and $+1.250 \pm 0.563$ μmol kg^{-1} decade^{-1} for the gridded and non-gridded data, respectively. These values resemble the results shown for the WSBW in the section plot of the time trends in C_T (Fig. 10A), providing confidence that the results are robust. No significant trends in (gridded or non-gridded) C_T are found in the three overlying water masses, although there is a hint at increase in the shallow waters (<200 m), notwithstanding seasonality and the upwelling character of the SHALLOW water mass at the defined 58°S–63°S latitude (Table 2).

The time trends in C^{TSR}_T (deemed to represent influences on C_T of natural variability) are not significantly different from zero in the three deeper water masses. This is deemed to confirm that there are no systematic time trends of hydrographic or biogeochemical origin over the 35 yr. The variability in C_T in the upper waters (Fig. 12; top panels of leftmost two columns), that likely is a result of uneven distribution of sampling in various seasons, is partly reproduced by C^{TSR}_T, suggesting that seasonality indeed obscures conceivable trends in C_T there.

The time trend of $C^{TSR}_{residual}$ (deemed to represent the time trend of C_{ant}) in the WSBW equals about one-third of that observed in measured C_T: 0.445 ± 0.405 μmol kg^{-1} decade^{-1}. This difference was also observed in the section plots of trends (Fig. 10A and D; text Section 6.1) and will be further discussed in text Section 7.3. The time trends in the other three water masses are not significantly different from 0. Finally, no increase in $C^{TSR}_{residual}$ is observed in the upper waters, suggesting very little penetration of C_{ant} into the upwelling waters.

6.3. Determined C^{TrOCA}_{ant}

The section of C_{ant} derived using the TrOCA method (Fig. 13) resembles the distribution of the concentration of (and trends in) CFC-12 (Fig. 8). Specifically, the low values in the WDW (circa 10 μmol kg^{-1}) and higher concentrations in two distinct bottom water cores (circa 16 μmol kg^{-1}) are clearly discernible in both properties. These values are in general accordance with earlier

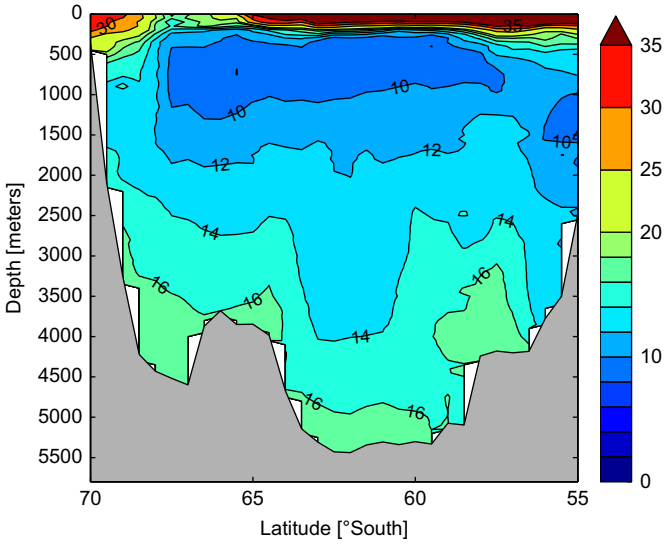

Fig. 13. Section plot of C_{ant} (μmol kg^{-1}) as determined with the TrOCA approach, valid for the year 2005. For the required input values of C_T, A^{MLR}_T, O_2, S, θ, phosphate and silicate we used the means of the cruises between 2002 and 2008 (see text Sections 5.7 and 6.3). All results are based on data that were adjusted for consistency in lWDW/uWSDW.

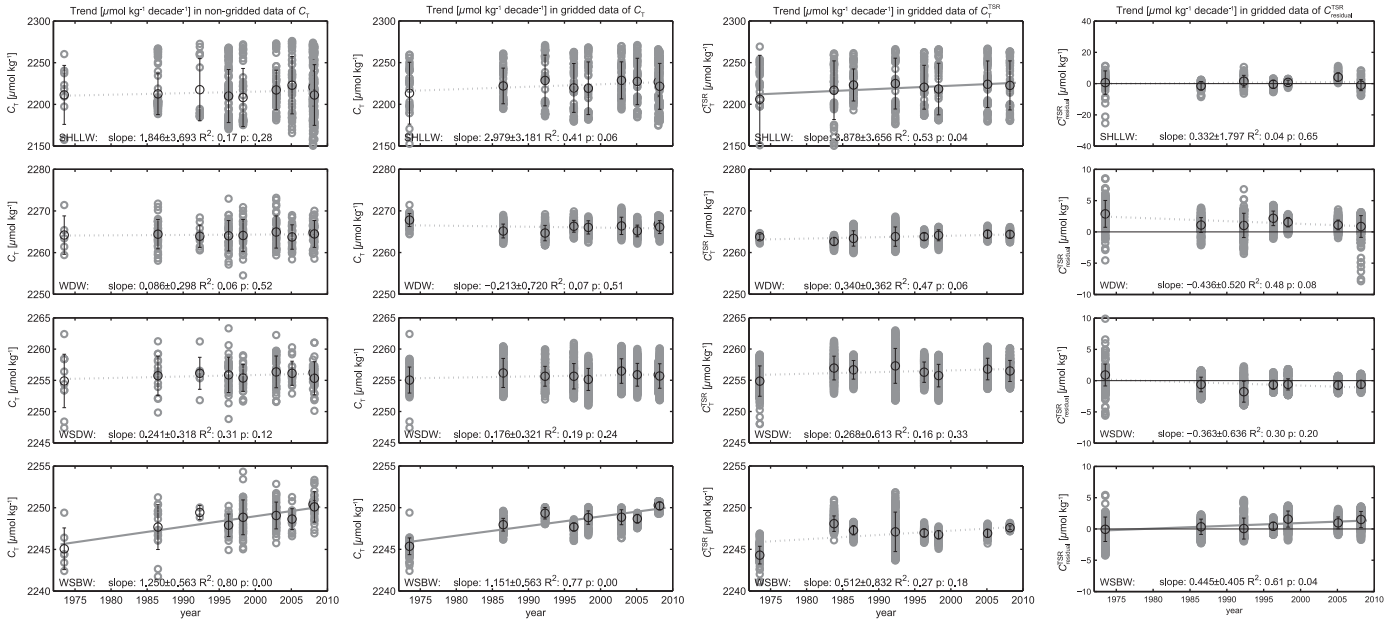

Fig. 12. Time trends (μmol kg^{-1} decade^{-1}) in the cores of four water masses (SHALLOW, WDW, WSDW, WSBW; see Table 2) computed using ordinary least squares regression. All results are based on data that were adjusted for consistency in lWDW/uWSDW. See Sections 5.6 and 6.2 for details. (A) non-gridded data of C_T; (B) gridded data of C_T; (C) C^{TSR}_T, the values of C_T predicted using a multivariate linear regression of the gridded C_T versus a suite of gridded independent parameters. These trends are deemed to represent the component of the variability in C_T that is attributable to natural variability; (D) $C^{TSR}_{residual}$, the residuals of the Time Series Residuals method, the trends through which are expected to reflect the component of the variability of gridded C_T that is due to uptake of C_{ant} at the ocean surface.

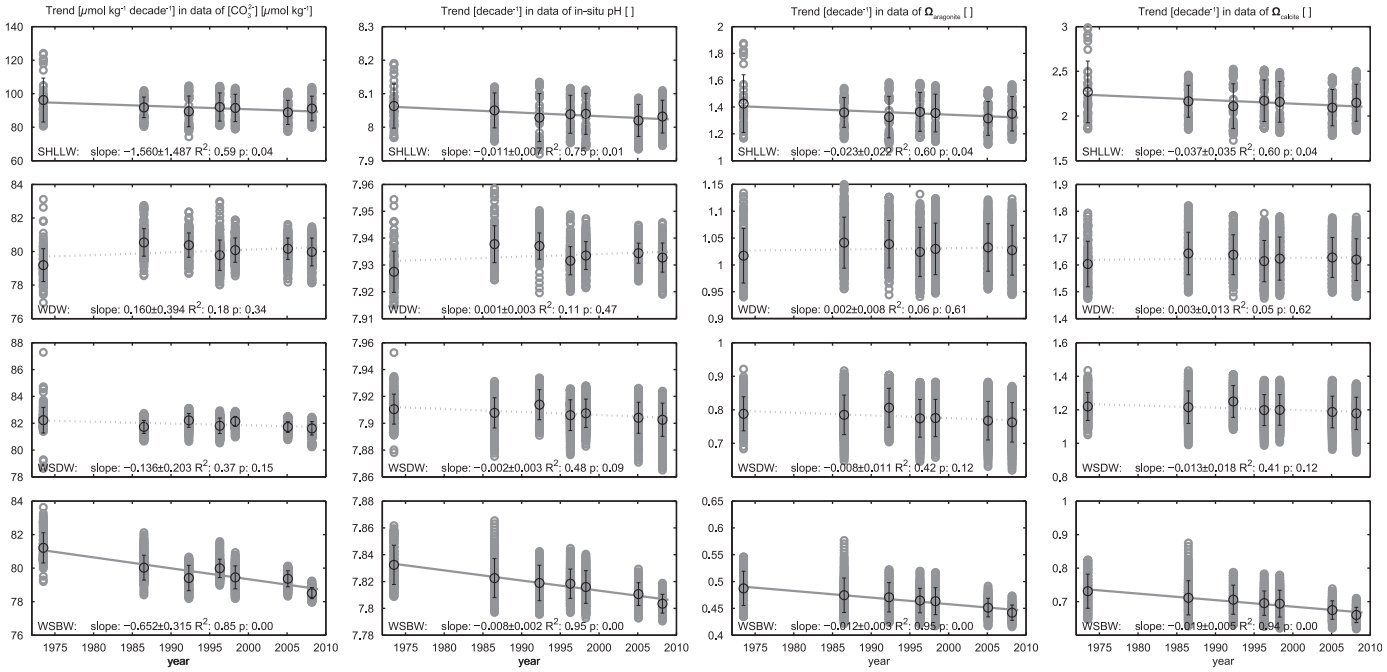

Fig. 14. Time trends in the cores of four water masses (SHALLOW, WDW, WSDW, WSBW; see Table 2), determined using ordinary least squares regression, of the calculated values of (A) the carbonate ion concentration [CO_3^{2-}]; (B) the concentration of hydroxide ion ([OH^-]), expressed as in situ pH (see text section 6.4); (C) the saturation state Ω of aragonite; (D) the saturation state Ω of calcite. Trends in (A) in μmol kg^{-1} $decade^{-1}$, trends in (B, C and D) in units of $decade^{-1}$. For the last two panels (C and D), values of Ω below 1 indicate that the seawater is undersaturated with respect to the aragonite or calcite crystalline state of $CaCO_3$, respectively. See Sections 5.8 and 6.4 for details. All results are based on data that were adjusted for consistency in lWDW/uWSDW.

published data (Lo Monaco et al., 2005b; Vázquez Rodríguez et al., 2009).

6.4. The carbonate system of the Weddell Gyre in a high-CO_2 world.

Significant decreasing time trends are observed for all calculated parameters of the carbonate system ([CO_3^{2-}], pH, Ω_{AR} and Ω_{CA}) in the shallow waters (<200 m; Table 2) and the WSBW (Fig. 14). For the shallow waters these trends exceed beyond the expected strong influence of seasonality there. In the WSBW, the time trend in the concentration of carbonate ion is -0.7 ± 0.3 μmol kg^{-1} $decade^{-1}$, which equates to almost -1% per decade. Orr et al. (2005) used a set of ocean carbon cycle models to predict the global evolution of [CO_3^{2-}] for the 2000–2100 era under a 'business-as-usual' scenario for anthropogenic emissions of CO_2. For the surface waters of the Southern Ocean, they computed an approximately linear trend of about -5 μmol kg^{-1} $decade^{-1}$ (their Fig. 5), resulting in aragonite undersaturation around the year 2065. That estimate is considerably more pronounced than the -1.6 ± 1.5 μmol kg^{-1} $decade^{-1}$ that we derive from measurements over the period 1973–2008, which would not result in undersaturation within the current century. Hauck et al. (2010), also note the projection of Orr et al. (2005) to be markedly higher than their own data-based estimates. However, we note here that 'shallow water' in the present study is defined to be located in, or close to, the upwelling region (cf. Table 2), and will therefore likely exhibit more modest rates of accumulation of C_{ant} compared to the rates in waters to the north and south of this region (Section 2), which the estimate of Orr et al. did include.

7. Discussion

This discussion contains a treatment of some of the uncertainties associated with the followed methodology, a comparison of our finding with earlier work, and an extrapolation of the results obtained at the Prime Meridian to the larger Weddell Gyre.

7.1. GEOSECS bias

The GEOSECS (1973) data are so far in the past compared to the 1984–2008 era of the other cruises that a conceivably remaining bias in the GEOSECS data will have excessive leverage in the linear regression. For example, if these data would, after the WDW normalization, still be 2 μmol kg^{-1} too low, time trends in C_T would be overestimated by about 25% (i.e., $+1.5$ instead of $+1.2$ μmol kg^{-1} $decade^{-1}$). We are confident, however, that any remaining bias in the GEOSECS is of limited influence on our results. Some justification for the used correction of -0.6 μmol kg^{-1} is found in the literature. Peng and Wanninkhof (2010) determined corrections for C_T for individual GEOSECS stations in the Atlantic Ocean. Their results indicate that C_T at the stations that are used in this study should be corrected by between 0 ± 4 μmol kg^{-1} (their Fig. 5) and -2 ± 4 μmol kg^{-1} (their Fig. 7). The fact that we observe a time trend in C_T also in the waters that were not sampled by GEOSECS (Figs. 5 and 10A) is an additional indication that the derived results are robust and not an artifact of GEOSECS bias.

7.2. Effects of WDW normalization

The absence of the trends in C_T in the WDW (Fig. 12, second row, first two columns) indicates that the normalization of values in the WDW was valid and effective. However, the spread that was observed in the WDW before normalization may have contained an obscured real-world trend. The detection of trends of CFC-12 hints at the slow but definite ventilation of this water mass. The trend in CFC-12 in the WDW is 0.041 ± 0.025 pmol kg^{-1} $decade^{-1}$, versus 0.138 ± 0.032 pmol kg^{-1} $decade^{-1}$ in the WSBW (see Table 5, Fig. 9). Translated to the results for C_{ant}, this suggests that the real-world trends in WSBW and WDW

conceivably may be as large as +1.65 and +0.49 μmol kg^{-1} decade^{-1}, respectively. However, the trend in non-adjusted data of C_T in the WSBW (excluding the strongly outlying data of ANT-V/2&3 and AJAX) is 1.1 ± 1.0 μmol kg^{-1} decade^{-1}, (i.e., less clearly resolved, but of similar slope as the adjusted data). Therefore, although we acknowledge the possibility that real-world trends in the WSBW might be up to 30% higher than the +1.2 ± 0.6 μmol kg^{-1} decade^{-1}, we opt not to perform such an upward correction of our results.

7.3. Attribution of trends

We show a distinct and unambiguous increase in C_T in the WSBW of about 1.2 ± 0.6 μmol kg^{-1} decade^{-1}. This trend is only partly consistent with the significant time trend in $C^{TSR}_{residual}$ (about 0.4 ± 0.4 μmol kg^{-1} decade^{-1}), deemed representative of an increase of C_{ant} over time. However, there is no significant time trend in the WSBW of C^{TSR}_T (0.512 ± 0.832 μmol kg^{-1} decade^{-1}), implying that there are no clear systematic time trends of biogeochemical and/or hydrographic origin over the 35 yr that would explain the remainder of the observed time trend in C_T. In order to more satisfyingly attribute the observed time trend in C_T to either natural variability or accumulation of anthropogenic CO_2, we consider below the alternative lines of evidence, and eventually opt to ascribe the entire increase of C_T (i.e., about 1.2 ± 0.6 μmol kg^{-1} decade^{-1}) for accumulation of anthropogenic CO_2 in the WSBW.

From an absence of trends in (lWDW/uWSDW-normalized) NO_3, PO_4 and O_2, we rule out enhanced remineralization as cause of the observed trend in C_T. Due to the limited accuracy of the A_T data and the lack of time trends in A^{MLR}_T (Section 5.4) no such statement can be made for the influence of $CaCO_3$ dissolution, but the rate of that process and the variability therein may be considered to be too small to suffice as an explanation (Sabine et al., 2002). Alternatively, part of the time trend in C_T in the WSBW might be the result of a changing formation process of the water mass. In order to explain the observed increasing temperature of the WSBW, Fahrbach et al. (2004) suggest that increases in the penetration of CDW into the Weddell Sea and in the amount of entrainment of (CDW-derived) WDW during the convective formation of WSBW from Ice Shelf Water (ISW) would increase the temperature of the WSBW. Lenton et al. (2009) provide a tentative mechanism for this increased penetration of CDW involving anthropogenically driven changes in atmospheric circulation. Such increased entrainment of WDW would inevitably also increase the C_T of the WSBW and can be quantified as follows. The WSBW is considered to be a mixture of Ice Shelf Water and near-continental slope WDW (ISW: $\theta = -1.85$ °C, salinity-normalized $C_T = 2250$ μmol kg^{-1}; WDW: $\theta = 0.25$ °C, salinity-normalized $C_T = 2285$ μmol kg^{-1}), with a gradient of the mixing line of 16.7 μmol kg^{-1} °C^{-1} (Hoppema et al., 1998). This gradient multiplied with the observed time trend of θ in the WSBW of +0.015 ± 0.006 °C decade^{-1} (comparable to the trend observed by Fahrbach et al., 2004) yields a time trend of C_T of 0.25 ± 0.10 μmol kg^{-1} decade^{-1}. In other words, an increase in the amount of WDW entrained by ISW during the formation of WSBW may at most explain ~20% of the observed trend in C_T.

Overall, we reckon that the observed increase of C_T in the WSBW at a rate of about 1.2 ± 0.6 μmol kg^{-1} decade^{-1} may best be completely ascribed to a true invasion of anthropogenic CO_2 into the deep Weddell Gyre. This attribution is at least partly supported by the significant time trend in $C^{TSR}_{residual}$ (0.4 ± 0.4 μmol kg^{-1} decade^{-1}). More importantly, the strong spatial correlation of the increase of C_T and the increase of CFC-12 (Fig. 11), is most convincing. However, the given rate of 1.151 ± 0.56 μmol kg^{-1} decade^{-1} is deemed to be an upper limit, because natural variability of hydrography may account for a part of the trend (0.25 ± 0.10 to 0.5 ± 0.8 μmol kg^{-1} decade^{-1}, as suggested above by the mixing consideration and the TSR approach, respectively).

7.4. Comparing the time trend of C_{ant} with other estimates

Hoppema et al. (2001), following the method of Poisson and Chen (1987), report a 'negligible' increase in C_{ant} between 1973 and 1998 from a comparison of cruise data from the mid-1990s with data of GEOSECS and AJAX. Although no significant change was determined, the authors concluded from statistical considerations that the increase of C_{ant} in the WSBW is almost certainly smaller than 2 μmol kg^{-1} decade^{-1}. That upper limit estimate is in agreement with the 1.2 ± 0.6 μmol kg^{-1} decade^{-1} found in the present study.

Another recent determination of ΔC_{ant} in the Weddell Sea, also along the 0°-meridian, relies on the eMLR method (Friis et al., 2005; see text Section 3.2.3) to derive an increase of C_{ant} between the two cruises ANT-X/4 (1992) and ANT-XXIV/2 (2008) (Hauck et al., 2010). The magnitude of the reported increases over 16 yr is similar to our findings. However, for individual water masses significant discrepancies exist with our results. Firstly, in the WSDW, the reported pronounced increase (~1.5–2.0 μmol kg^{-1} over 16 yr), is incompatible with the about fivefold smaller and non-significant time trend in C_T found in our study (0.2 ± 0.3 μmol kg^{-1} decade^{-1}; Fig. 12, Table 5). Moreover, we do not find a significant time trend of $C^{TSR}_{residual}$ (−0.4 ± 0.6 μmol kg^{-1} decade^{-1}; Fig. 12, Table 5) either, representative of C_{ant}. In favor of the findings of Hauck et al., one might argue that the procedure of WDW normalization performed in the present study has inadvertently also removed the trend in the WSDW. However, that argument is mutually exclusive with our concurrent finding of a significant positive trend in C_T in the WSBW (about +1.2 ± 0.6 μmol kg^{-1} decade^{-1}), where Hauck et al. report an increase that is significantly smaller than 1 μmol kg^{-1} over 16 yr. On the other hand, the reported low increase in the WSBW *does* coincide with our TSR-based results for $C^{TSR}_{residual}$ (WSBW +0.4 ± 0.4 μmol kg^{-1} decade^{-1}). However, we do not hold this resemblance to demonstrate the veracity of the results of either study, mainly in light of the fact that the two studies indicate different water masses to dominate the storage of C_{ant} (namely, WSDW in the study of Hauck et al., and WSBW in the present study). Instead, the discrepancies between the two studies may be due to the fact that the used datasets are not the same. Specifically, although Hauck et al. (2010) showed the overall quality of the used data to be satisfactory, we have chosen to exclude the southerly deep C_T measurements (south of 63°S and deeper than 1500 m) of the ANT-X/4 (1992) cruise, which we consider to be erroneously high by up to 7 μmol kg^{-1} on the basis of a regression versus θ (see above Section 5.1). The exclusion we performed (and the additional exclusion of C_T measurements of AJAX, 1983) is corroborated by the distribution of time trends in our remaining database of actually measured C_T (Fig. 10A), which closely resembles the distribution of time trends of CFC-12 in the deep region of the Weddell Gyre (Section 6.1; Fig. 8C), comprising the WSDW and WSBW. In the study of Hauck et al., the presence of a bias in part of the data may have led to increased uncertainty (but not necessarily inaccuracy) in the applied MLR and the results derived from it. Additionally, the low number of samples qualifying as WSBW in the study of Hauck et al. (Fig. 5) may have affected their results obtained for this water mass.

7.5. The concentration of C_{ant} derived from the observed decadal time trend

The Transient Steady State approach (Tanhua et al., 2007; Section 3.1.5) implies that the per decade increase in C_{ant}

represents a fraction of about 0.2 ± 0.03 of the total concentration of C_{ant} (i.e., C_{ant} [μmol kg^{-1}] $\approx 5 \cdot \Delta C_{ant}$ [μmol kg^{-1} decade^{-1}]; notice the informal use of units in this expression). Assuming that the time trend of C_{ant} in the WSBW equals that of C_T (i.e., about 1.2 ± 0.6 μmol kg^{-1} decade^{-1}), we infer a C_{ant} of 6 ± 3 μmol kg^{-1}. We will take 1995 as the year for which this estimate is valid, that is, slightly more recent than the midpoint of the 1973–2008 period. The error bound of this estimate is not formally determined, due to several assumptions inherent to the taken approach. Nonetheless, the estimate may serve as a rough guide to assess the validity of our study versus various other estimates of C_{ant} previously reported by other investigators.

Table 6 lists the C_{ant} estimates derived in this study, as well as various estimates of the concentration of C_{ant} in the Weddell Gyre that were obtained by other investigators (Poisson and Chen, 1987; Lo Monaco et al., 2005b; Waugh et al., 2006; Vázquez-Rodríguez et al., 2009). Poisson and Chen (1987), using a back-calculation approach (Section 3.1.1), reported a concentration of C_{ant} in the deep Weddell Sea (for 1984) of circa 6 ± 5 μmol kg^{-1}, which is in agreement with the results of this study. However, several estimates of C_{ant} in the WSBW that have been derived using the ΔC^* method are close to zero (Sabine et al., 2004; Waugh et al., 2006; Vázquez-Rodríguez et al., 2009). On the other hand, results from application of the TTD approach (e.g., Waugh et al., 2006; Vázquez-Rodríguez et al., 2009) are generally somewhat higher than our results. Both authors report estimates of C_{ant} in the WDW and the (largely WSDW-derived) AABW at 30°E of about 9 μmol kg^{-1}. These estimates are significantly higher (WDW) or slightly higher (AABW) than the results obtained in the present study (0 and 6 ± 3 μmol kg^{-1}, respectively). On the other hand, by assuming an undersaturation of dissolved oxygen of 12%, Lo Monaco et al. (2005a, 2005b) used the C_T^0 method to determine a C_{ant} concentration in 1996 of circa 22 μmol kg^{-1} in the core of the AABW at 30°E. This estimate is very significantly higher than what is obtained in our study using the Transient Steady State method.

Results of the applications of the TrOCA method agree fairly well between the different studies, which is not surprising given the strict definition and application of the method. However, all TrOCA-based estimates for the WSBW (or AABW) (all around 15 μmol kg^{-1}) are higher than results obtained by our study or by studies employing the TTD or ΔC^* methods.

Obviously, the highest of the above discussed, previously published estimates of C_{ant} for the WSBW/AABW presented in Table 6, are incompatible with the results of this study. We here assume the central argument of the Transient Steady State method to be valid. That is, the exponential accumulation of C_{ant} in the atmosphere and the ocean surface will lead to exponentially increasing concentrations in the ocean interior (Tanhua et al., 2007). The time trends in C_{ant} that would therefore necessarily be associated with high concentrations of C_{ant} (for example, a C_{ant} of $\sim$20 μmol kg^{-1} requires a trend in C_{ant} of $\sim$4 μmol kg^{-1} decade^{-1}) are irreconcilable with the observed time trends in measured C_T (about $+1.2 \pm 0.6$ μmol kg^{-1} decade^{-1}). Moreover, the trends in C_T observed in our study are deemed to represent an upper limit of the trend in C_{ant} (see text Section 7.3), which further reduces the likelihood that the highest previously published estimates of C_{ant} in Table 6 are accurate.

7.6. *The rate of increase of the inventory of C_{ant} of the deep Weddell Gyre.*

The determined time trend in the concentration of C_{ant} along the section may be spatially extrapolated and integrated to obtain

Table 6
Comparison of several estimates of C_{ant} from previously published literature. Reproduced values necessarily are simplified from originally reported depth profiles and section plots. Many of these estimates are from data obtained along the section at 30°E (WOCE section I06), that is located at the eastern-most extent of the Weddell Gyre (as indicated in the column 'longitude of section'), and thus do not cover the exact same water masses as the present study. Most notably, the composition of the bottom water at 30°E (Antarctic Bottom Water, AABW) is alike (and largely derived from) the WSDW, rather than WSBW. Although the AABW at 30°E to some extent is formed in areas to the East of the Weddell Sea, the involved formation processes are likely comparable, and since significant mixing and horizontal homogenization takes place in the Southern Ocean, and CFC-12 concentrations are comparable (data not shown), we consider the comparison between results from these two sections not perfect but informative.

Source	C_{ant} estimate (μmol kg^{-1})	Nominal year	Longitude of section	Method	Remarks
Warm Deep Water					
Lo Monaco et al. (2005a)	~6	1996	30°E	C_T^0 (assuming O_2 saturation)	From their Fig. 5A
Lo Monaco et al. (2005a)	~9	1996	30°E	C_T^0 (assuming 12% O_2 undersaturation)	From their Fig. 5B
Sabine et al. (2004)	~0	1996	30°E	ΔC^*	From GLODAP data product
Lo Monaco et al. (2005b)	~6	1996	30°E	ΔC^* (assuming 12% O_2 undersaturation)	From their Fig. 4C
Waugh et al. (2006)	~0	1996	30°E	ΔC^*	From their Fig. 6B
Vázquez-Rodríguez et al. (2009)	~1	1996	30°E	ΔC^*	From their Fig. 4
Waugh et al. (2006)	~8	1996	30°E	TTD	From their Fig. 6B
Vázquez-Rodríguez et al. (2009)	~10	1996	30°E	TTD	From their Fig. 4
Lo Monaco et al. (2005b)	~10	1996	30°E	TrOCA	From their Fig. 4A
Vázquez-Rodríguez et al. (2009)	~7	1996	30°E	TrOCA	From their Fig. 4
This study	~9	2005	0°E	TrOCA	Text Sections 5.7 and 6.3
This study	0	1995	0°E	A *priori* assumption	Text Section 5.1
WSBW/AABW					
Poisson and Chen (1987)	6 ± 5	1984	0°E	Diff. of C_T^0 between WDW and WSBW	
Lo Monaco et al. (2005a)	~8	1996	30°E	C_T^0 (assuming O_2 saturation)	From their Fig. 5A
Lo Monaco et al. (2005a)	~22	1996	30°E	C_T^0 (assuming 12% O_2 undersaturation)	From their Fig. 5B
Sabine et al. (2004)	~0	1996	30°E	ΔC^*	From GLODAP data product
Lo Monaco et al. (2005b)	~18	1996	30°E	ΔC^* (assuming 12% O_2 undersaturation)	From their Fig. 4C
Waugh et al. (2006)	~0	1996	30°E	ΔC^*	From their Fig. 6B
Vázquez-Rodríguez et al. (2009)	~1	1996	30°E	ΔC^*	From their Fig. 4
Waugh et al. (2006)	~9	1996	30°E	TTD	From their Fig. 6B
Vázquez-Rodríguez et al. (2009)	~8	1996	30°E	TTD	From their Fig. 4
Lo Monaco et al. (2005b)	~15	1996	30°E	TrOCA	From their Fig. 4A
Vázquez-Rodríguez et al. (2009)	~13	1996	30°E	TrOCA	From their Fig. 4
This study	~16	2005	0°E	TrOCA	Text Sections 5.7 and 6.3
This study	6 ± 3	1995	0°E	From time trend in C_T (using TSS)	Text Section 7.5

a first estimate of the time trend of the inventory of C_{ant} in the deep (below 3000 m) Weddell Gyre over the period of this study (i.e., 1973–2008), as follows. The mean rate of increase in C_T (taken to represent an upper bound to rate of increase of C_{ant}, see Section 7.3) of all grid points along the section between 70°S and 55°S and below 3000 m depth is 0.9 ± 0.4 μmol kg^{-1} decade^{-1}. Assuming this rate of increase of the concentration to be representative of the deep Weddell Gyre as a whole (here taken as west of 20°E and deeper than 3000 m, and thus having a volume of approximately 11×10^6 km^3), the rate of increase of the inventory of C_{ant} in the deep (below 3000 m) Weddell Gyre is calculated to be about 12 ± 6 10^{12} gC yr^{-1} (TgC yr^{-1}), which is about 0.15 ± 0.07% of the current rate of anthropogenic emissions. Please note that this rate of local storage of C_{ant} does not include the additional C_{ant} transferred into other oceans with the northeastward spreading AABW. Moreover, the storage of C_{ant} in the shallower layers (typically <200 m), that actually have the highest C_{ant} component, could not be included in this approximation due to seasonal variability.

The calculated rate of storage of C_{ant} in the deep Weddell Gyre appears to be compatible with the results of Anderson et al. (1991), who estimated an export of C_{ant} from the continental shelf into the deep Weddell Gyre of 8–16 TgC year^{-1} from observations in the Filchner Depression in the southern Weddell Sea in 1988–1989. The latter rate of export would on the one hand include the transfer with AABW into other oceans, yet on the other hand, just as in our study exclude the shallower layers.

8. Conclusions

Time trends in the concentration of C_T were determined directly from measured values along the 0°-meridian in the Weddell Gyre in the Southern Ocean. A significant positive trend in C_T of $+1.2 \pm 0.6$ μmol kg^{-1} decade^{-1} is determined in the WSBW. The determined time trends in back-calculated preformed C_T (C_T^0) appear affected by inaccuracies of the oxygen data. Within the observed trend in C_T, we attempted to separate the contributions of natural variability and the uptake of anthropogenic CO_2 from the atmosphere, by use of a novel MLR-based technique: Time Series Residuals (TSR). In the taken approach, trends in the residuals ($C_{residual}^{TSR}$) of an MLR encompassing all data of 10 cruises are assumed to represent the anthropogenic component of the observed trends in C_T, whereas trends in the MLR-predicted C_T values (C_T^{TSR}) are assumed to reflect natural variability in C_T. Use of this approach regrettably did not allow for a convincing attribution of the observed time trend in measured data of C_T to either natural variability or uptake of anthropogenic CO_2 from the atmosphere.

However, the significant resemblance between the spatial distributions of time trends determined in C_T and CFC-12 provides compelling evidence that the results reflect genuine changes in C_T of the deep Weddell Gyre that are propagated from the surface into the interior. From a consideration of the formation process of the WSBW and observed temperature changes of that water mass, we rule out a strong influence on the observed time trend in C_T of variable entrainment of WDW into the forming WSBW, thereby strengthening the case for an anthropogenic (rather than a hydrographic) origin of the observed increases in C_T in the deep Weddell Gyre. If indeed assuming the trend in C_{ant} to equal the trend in C_T (i.e., the trend in C_{ant} equals about $+1.2 \pm 0.6$ μmol kg^{-1} decade^{-1}), and further assuming an exponential buildup of C_{ant} in the deep ocean (as in the atmosphere and surface ocean), we calculate a total concentration of C_{ant} in the WSBW of 6 ± 3 μmol kg^{-1} for the year 1995. This estimate is significantly lower than estimates obtained with the TrOCA method, but higher than what is generally obtained using the ΔC^* method. Results from investigators using the TTD method compare more favorably with our estimate. Extrapolating the determined rate of increase of the concentration of C_{ant} to the deep Weddell Gyre as a whole (below 3000 m, west of 10°E), we obtain a rate of increase of the inventory of C_{ant} of about 12 ± 6 TgC yr^{-1} for 1995, or about 0.15% of current anthropogenic emissions to the atmosphere. This case study of the Weddell Gyre demonstrates the value of the direct determination of time trends of C_T in the deep ocean.

9. Recommendations for future research

While we arguably have been successful in using historical data of C_T to determine time trends in the deep Weddell Sea, we experienced difficulties in separating the natural and anthropogenic components of the observed changes, whether with the proposed TSR method or the classical C_T^0 approach. In part, this was due to uncertainties about the accuracy of the ancillary parameters required for such an exercise. Dataset compilation efforts like GLODAP and CARINA may to some extent eliminate systematic cruise biases of these properties. Nevertheless it has become obvious that further improvement of the original measurements is needed in future cruises. Variable biases of up to 3% are quite common in the used datasets of nutrients and dissolved O_2, while in fact the state-of-the-art does permit an order of magnitude lower uncertainty (i.e., circa 0.2%), approaching what is common nowadays for C_T and A_T. Reference standards for measurements of the major nutrients are being developed and made available to the international community under the flag of the Meteorological Research Institute, Tsukuba, Japan (Aoyama et al., 2008). The determination of the increase of inventories of C_T and the separation of the natural and anthropogenic components of this increase will likely benefit greatly from the widespread adoption of these reference materials. The development of reference material (or another method of standardization) for dissolved oxygen would similarly be of great benefit. A simple standardization method for oxygen exists, namely, the measurement of seawater saturated with oxygen at stable temperature and air pressure conditions, where the oxygen concentration is known from the theoretical solubility (Reinthaler et al., 2006). Analysts are encouraged to use this method until reference material becomes available.

The further long term pursuance of repeated interior ocean measurements of CO_2, ideally accompanied by continued measurements of CFCs and the broad adoption of SF_6 as an additional anthropogenic tracer, will be crucial for further constraining the oceanic uptake and storage of anthropogenic CO_2 on decadal time scales, both locally in the Weddell Gyre and in the ocean at large.

Acknowledgments

The diligent work performed by the officers, crew and scientists that participated in the many expeditions of which results are used in this study is immensely appreciated. Without this measurement effort, sustained over more than three decades already, this work would not have been possible. The excellent cooperation with the officers, crew and scientific party during *PFS Polarstern* expedition ANT-XXIV/3 is specifically acknowledged. Valuable suggestions by two anonymous reviewers have helped to substantially improve this manuscript.

Appendix A. Supplementary material

Supplementary data associated with this article can be found in the online version at doi:10.1016/j.dsr2.2011.08.007.

References

Anderson, L.G., Holby, O., Lindegren, R., Ohlson, M., 1991. The transport of anthropogenic carbon dioxide into the Weddell Sea. J. Geophys. Res. 96, 16679–16687.

Anderson, L.A., Sarmiento, J.L., 1994. Redfield ratios of remineralization determined by nutrient data-analysis. Global Biogeochem. Cycles 8, 65–80.

Aoyama, M., Barwell-Clarke, J., Becker, S., Blum, M., Braga, E.S., Coverly, S.C., Czobik, E., Dahllof, I., Dai, M.H., Donnell, G.O., Engelke, C., Gong, G.C., Gi-Hoon Hong, Hydes, D.J., Jin, M.M., Kasai, H., Kerouel, R., Kiyomono, Y., Knockaert, M., Kress, N., Krogslund, K.A., Kumagai, M., Leterme, S., Yarong, Li, Masuda, S., Miyao, T., Moutin, T., Murata, A., Nagai, N., Nausch, G., Ngirchechol, M.K., Nybakk, A., Ogawa, H., van Ooijen, J., Ota, H., Pan, J.M., Payne, C., Pierre-Duplessix, O., Pujo-Pay, M., Raabe, T., Saito, K., Sato, K., Schmidt, C., Schuett, M., Shammon, T.M., Sun, J., Tanhua, T., White, L., Woodward, E.M.S., Worsfold, P., Yeats, P., Yoshimura, T., Youenou, A., Zhang, J.Z., 2008. 2006 Intercomparison Exercise for Reference Material for Nutrients in Seawater in a Seawater Matrix. Technical Reports of the Meteorological Research Institute No. 58, 104 pp.

Bainbridge, A.E. (Ed.), 1981. GEOSECS Atlantic Expedition, vol. 1, Hydrographic Data 1972–1973, IDOE/ NSF, 121 pp.

Bakker, D.C.E, Hoppema, M., Schroeder, M., Geibert, W., de Baar, H.J.W., 2008. A rapid transition from ice covered CO_2-rich waters to a biologically mediated CO_2 sink in the eastern Weddell Gyre. Biogeosciences 5, 1373–1386.

Behrendt, A., Fahrbach, E., Hoppema, M., Rohardt, G., Boebel, O., Klatt, O., Wisotzki, A., Witte, H., 2011. Variations of Winter Water properties and sea ice along the Greenwich meridian on decadal time scales. Deep-Sea Res. II 58, 2524–2532.

Brewer, P.G., Goldman, J.C., 1976. Alkalinity changes generated by phytoplankton growth. Limnol. Oceanogr. 21 (1), 108–117.

Brewer, P.G, 1978. Direct observation of the oceanic CO_2 increase. Geophys. Res. Lett. 5, 997–1000.

Broecker, W., 1974. "NO", a conservative water-mass tracer. Earth Planet. Sci. Lett. 23, 100–107.

Chen, C.T., Millero, F.J., 1979. Gradual increase of oceanic CO_2. Nature 277, 205–206.

Chen, C.T.A., 1993. The oceanic anthropogenic CO_2 sink. Chemosphere 27 (6), 1041–1064.

Chipman, D.W., Takahashi, T., Sutherland, S.C., 1986. Carbon chemistry of the South Atlantic Ocean and the Weddell Sea: The results of the Atlantic Long Lines (AJAX) Expeditions, October, 1983–February, 1984. Lamont-Doherty Geological Observatory, Columbia University, Palisades, NY, 185 pp.

Deacon, G.E.R., 1984. The Antarctic Circumpolar Ocean. Cambridge University Press, Cambridge, New York.

Dickson, A., 2001. Reference material for oceanic CO_2 measurements. Oceanography 14, 21–22.

Dickson, A.G., Sabine, C.L., Christian, J., 2007. Guide to Best Practices for Ocean CO_2 Measurements, 3. PICES Special Publication, 191 pp.

Fahrbach, E., Hoppema, M., Rohardt, G., Schröder, M., Wisotzki, A., 2004. Decadal-scale variations of water mass properties in the deep Weddell Sea. Ocean Dyn. 54, 77–91.

Fahrbach, E., de Baar, H.J.W. (Eds.), 2010. The Expedition of the Research Vessel 'Polarstern' to the Antarctic in 2008 (ANT-XXIV/3). Reports on Polar and Marine Research 606, 232 pp. hdl:10013/epic.34050.

Fahrbach, E., Hoppema, M., Rohardt, G., Boebel, O., Klatt, O., Wisotzki, A., 2011. Warming of deep and abyssal water masses along the Greenwich meridian on decadal time sacles: the Weddell gyre as a heat buffer. Deep-Sea Res. II 58, 2509–2523.

Feely, R.A., Sabine, C.L., Lee, K., Berelson, W., Kleypas, J., Fabry, V.J., Millero, F.J., 2004. Impact of anthropogenic CO_2 on the $CaCO_3$ system in the oceans. Science 305, 362–366.

Fine, R.A., 2011. Observations of CFCs and SF_6 as Ocean Tracers. Annu. Rev. Mar. Sci. 3, 173–195.

Foster, T., Carmack, E., 1976. Temperature and salinity structure in the Weddell Sea. J. Phys. Oceanogr. 6, 36–44.

Friis, K., Körtzinger, A., Pätsch, J., Wallace, D.W.R., 2005. On the temporal increase of anthropogenic CO_2 in the subpolar North Atlantic. Deep-Sea Res. I 52, 681–698.

Gammon, R.H., Cline, J., Wisegarver, D., 1982. Chlorofluoromethanes in the Northeast Pacific Ocean: measured vertical distributions and application as transient tracers of upper ocean mixing. J. Geophys. Res. 87 (C12), 9441–9454.

Geibert, W., Assmy, P., Bakker, D.C.E., Hanfland, C., Hoppema, M., Pichevin, L.E., Schroeder, M., Schwarz, J.N., Stimac, I., Usbeck, R., Webb, A., 2010. High productivity in an ice melting hot spot at the eastern boundary of the Weddell Gyre. Global Biogeochem. Cycles 24, GB3007.

Gruber, N., Sarmiento, J.L., Stocker, T., 1996. An improved method for detecting anthropogenic CO_2 in the oceans. Global Biogeochem. Cycles 10, 809–837.

Hall, T.M., Haine, T.W.N., Waugh, D.W., 2002. Inferring the concentration of anthropogenic carbon in the ocean from tracers. Global Biogeochem. Cycles 4, 1131.

Hall, T.M., Waugh, D.W., Haine, T.W.N., Robbins, P.E., Khatiwala, S., 2004. Estimates of anthropogenic carbon in the Indian Ocean with allowance for mixing and time-varying air–sea CO_2 disequilibrium. Global Biogeochem. Cycles 18, GB1031.

Hauck, J., Hoppema, M., Bellerby, R.G.J., Völker, C., Wolf-Gladrow, D., 2010. Data-based estimation of anthropogenic carbon and acidification in the Weddell Sea on a decadal timescale. J. Geophys. Res. 115, C03004.

Hoppema, M., Fahrbach, E., Schröder, M., Wisotzki, A., de Baar, H.J.W., 1995. Winter-summer differences of carbon dioxide and oxygen in the Weddell Sea surface layer. Mar. Chem. 51, 177–192.

Hoppema, M., Fahrbach, E., Stoll, M.H.C., de Baar, H.J.W., 1998. Increase of carbon dioxide in the bottom water of the Weddell Sea, Antarctica. Mar. Chem. 59, 201–210.

Hoppema, M., Klatt, O., Roether, W., Fahrbach, E., Bulsiewicz, K., Rodehacke, C., Rohardt, G., 2001. Prominent renewal of Weddell Sea Deep Water from a remote source. J. Mar. Res. 59, 257–279.

Hoppema, M., 2004. Weddell Sea as a globally significant contributor to deep-sea sequestration of natural carbon dioxide. Deep-Sea Res. I 51, 1169–1177.

Hoppema, M., Middag, R., de Baar, H.J.W., Fahrbach, E., van Weerlee, E.M., Thomas, H., 2007. Whole season net community production in the Weddell Sea. Polar Biol. 31, 101–111.

Huhn, O., Hellmer, H., Rhein, M., Rodehacke, C., Roether, W., Schodlock, M.P., Schröder, M., 2008. Evidence of deep- and bottom-water formation in the western Weddell Sea. Deep-Sea Res. II 55, 1098–1116.

Johnson, K.M., Wills, K.D., Butler, D.B., Johnson, W.K., Wong, C.S., 1993. Coulometric total carbon dioxide analysis for marine studies—maximizing the performance of an automated gas extraction system and coulometric detector. Mar. Chem. 44 (2–4), 167–187.

Keeling, C.D., 1960. The concentration and isotopic abundances of carbon dioxide in the atmosphere. Tellus 12 (2), 200–203.

Key, R.M., Kozyr, A., Sabine, C.L., Lee, K., Wanninkhof, R., Bullister, J.L., Feely, R.A., Millero, F.J., Mordy, C., Peng, T.H., 2004. A global ocean carbon climatology: results from Global Data Analysis Project (GLODAP). Global Biogeochem. Cycles 18, GB4031.

Key, R.M., Tanhua, T., Olsen, A., Hoppema, M., Jutterström, S., Schirnick, C., van Heuven, S., Kozyr, A., Lin, X., Velo, A., Wallace, D.W.R., Mintrop, L., 2010. The CARINA data synthesis project: Introduction and overview. Earth Syst. Sci. Data 2, 105–121.

Khatiwala, S., Visbeck, M., Schlosser, P., 2001. Age tracers in an ocean GCM. Deep-Sea Res. I 48 (6), 1423–1441.

Klatt, O., Roether, W., Hoppema, M., Bulsiewicz, K., Fleischmann, U., Rodehacke, C., Fahrbach, E., Weiss, R.F., Bullister, J.L., 2002. Repeated CFC sections at the Greenwich Meridian in the Weddell Sea. J. Geophys. Res. 107, C3030.

Klatt, O., Fahrbach, E., Hoppema, M., Rohardt, G., 2005. The transport of the Weddell Gyre across the Prime Meridian. Deep-Sea Res. II 52, 513–528.

Körtzinger, A., Mintrop, L., Duinker, J.C., 1998. On the penetration of anthropogenic CO_2 into the North Atlantic Ocean. J. Geophys. Res. 103 (C9), 18689.

Lenton, A., Codron, F., Bopp, L., Metzl, N., Cadule, P., Tagliabue, A., LeSommer, J., 2009. Stratospheric ozone depletion reduces ocean carbon uptake and enhances ocean acidification. Geophys. Res. Lett. 36, L12606.

Levine, N., Doney, S., Wanninkhof, R., Lindsay, K., Fung, I.Y., 2008. Impact of ocean carbon system variability on the detection of temporal increases in anthropogenic CO_2. J. Geophys. Res. 113, C03019.

Lo Monaco, C., Metzl, N., Poisson, A., Brunet, C., Schauer, B., 2005a. Anthropogenic CO_2 in the Southern Ocean: Distribution and inventory at the Indian-Atlantic boundary (World Ocean Circulation Experiment line I6). J. Geophys. Res. 110, C06010.

Lo Monaco, C., Goyet, C., Metzl, N., Poisson, A., Touratier, F., 2005b. Distribution and inventory of anthropogenic CO_2 in the Southern Ocean: comparison of three data-based methods. J. Geophys. Res. 110, C09502.

Matear, R.J., McNeil, B.I., 2003. Decadal accumulation of anthropogenic CO_2 in the Southern Ocean: a comparison of CFC-age derived estimates to multiple-linear regression estimates. Global Biogeochem. Cycles 17 (4), 1113.

Matsumoto, K., Gruber, N., 2005. How accurate is the estimation of anthropogenic carbon in the ocean? An evaluation of the ΔC^* method. Global Biogeochem. Cycles 19, GB3014.

McNeil, B.I., Matear, R.J., Tilbrook, B., 2001. Does carbon-13 track anthropogenic CO_2 in the Southern Ocean? Global Biogeochem. Cycles 15, 597–613.

McNeil, B.I., Matear, R.J., Key, R., Bullister, J., Sarmiento, J., 2003. Anthropogenic CO_2 uptake by the ocean based on the global chlorofluorocarbon data set. Science 299, 235–239.

Metzl, N., 2009. Decadal increase of oceanic carbon dioxide in Southern Indian Ocean surface waters (1991–2007). Deep-Sea Res. II 56, 607–619.

Millero, F.J., Woosley, R., DiTrolio, B., Waters, J., 2009. The effect of ocean acidification on the speciation of metals in natural waters. Oceanography 22, 72–85.

Mintrop, L., Perez, F.F., Gonzalez-Davila, M., Santana-Casiano, M.J., Kortzinger, A., 2000. Alkalinity determination by potentiometry: intercalibration using three different methods. Cienc. Mar. 26 (1), 23–37.

Olafsson, J., Olafsdottir, S.R., Benoit-Cattin, A., Danielsen, M., Arnarson, T.S., Takahashi, T., 2009. Rate of Iceland Sea acidification from time series measurements. Biogeosciences 6, 2661–2668.

Olsen, A., Omar, A.M., Bellerby, R.G.J., Johannessen, T., Ninnemann, U., Brown, K.R., Olsson, K.A., Olafsson, J., Nondal, G., Kivimäe, C., Kringstad, S., Neill, C., Olafsdottir, S., 2006. Magnitude and origin of the anthropogenic CO_2 increase and ^{13}C Suess effect in the Nordic seas since 1981. Global Biogeochem. Cycles 20, 1–12.

Orr, J.C., Fabry, V.J., Aumont, O., Bopp, L., Doney, S.C., Feely, R.A., Gnanadesikan, A., Gruber, N., Ishida, A., Joos, F., Key, R.M., Lindsay, K., Maier-Reimer, E., Matear, R.J., Monfray, P., Mouchet, A., Najjar, R.G., Plattner, G.-K., Rodgers, K.B., Sabine, C.L., Sarmiento, J.L., Schlitzer, R., Slater, R.D., Totterdell, I.J., Weirig, M.-F., Yamanaka, Y., Yool, A., 2005. Anthropogenic ocean acidification over the

twenty-first century and its impact on calcifying organisms. Nature 437, 681–686.
Peacock, S., Maltrud, M., 2006. Transit-time distributions in a global ocean model. J. Phys. Oceanogr. 36 (3), 474–495.
Peng, T., Wanninkhof, R., Bullister, J., Feely, R.A., Takahashi, T., 1998. Quantification of decadal anthropogenic CO_2 uptake in the ocean based on dissolved inorganic carbon measurements. Nature 396, 560–563.
Peng, T., Wanninkhof, R., Feely, R.A., 2003. Increase of anthropogenic CO_2 in the Pacific Ocean over the last two decades. Deep-Sea Res. II 50, 3065–3082.
Peng, T., Wanninkhof, R., 2010. Increase in anthropogenic CO_2 in the Atlantic Ocean in the last two decades. Deep-Sea Res. I 57 (6), 755–770.
Pérez, F.F, Vázquez-Rodríguez, M., Louarn, E., Padin, X.A., Mercier, H., Ríos, A.F., 2008. Temporal variability of the anthropogenic CO_2 storage in the Irminger Sea. Biogeosciences 5, 1669–1679.
Pérez, F.F., Vázquez-Rodríguez, M., Mercier, H., Velo, A., Lherminier, P., Ríos, A.F., 2010. Trends of anthropogenic CO_2 storage in North Atlantic water masses. Biogeosciences 7, 1789–1807.
Postma, H., 1964. The exchange of oxygen and carbon dioxide between the ocean and the atmosphere. Neth. J. Sea Res. 2 (2), 258–283.
Poisson, A., Chen, C.T.A., 1987. Why is there little anthropogenic CO_2 in the Antarctic Bottom Water? Deep-Sea Res. A 34, 1255–1275.
Redfield, A.C., Ketchum, B.H., Richards, F.A., 1963. The influence of organisms on the composition of sea-water. In: Hill, M.N. (Ed.), The Composition of Seawater. Comparative and Descriptive OceanographyHarvard University Press.
Reinthaler, T., Bakker, K., Manuels, R., van Ooijen, J., Herndl, G.J., 2006. Fully automated spectrophotometric approach to determine oxygen concentrations in seawater via continuous-flow analysis. Limnol. Oceanogr.: Methods 4, 358–366.
Sabine, C.L., Key, R.M., Johnson, K., Millero, F.J., Poisson, A., Sarmiento, J.L., Wallace, D.W.R., 1999. Anthropogenic CO_2 inventory of the Indian Ocean. Global Biogeochem. Cycles 13, 179–198.
Sabine, C., Key, R., Feely, R., Greeley, D., 2002. Inorganic carbon in the Indian Ocean: distribution and dissolution processes. Global Biogeochem. Cycles 16 (4), 1067.
Sabine, C.L., Feely, R.A., Gruber, N., Key, R., Lee, K., Bullister, J.L., 2004. The oceanic sink for anthropogenic CO_2. Science 305, 367–371.
Sabine, C.L., Feely, R.A., Millero, F.J., Dickson, A.G., Langdon, C., Mecking, S., Greeley, D., 2008. Decadal changes in Pacific carbon. J. Geophys. Res. 113, C07021.
Schnack-Schiel, S. (Ed.), 1987. The Winter-Expedition of the Research Vessel 'Polarstern' to the Antarctic (ANT V/1-3). Reports on Polar Research 39, 259 pp.
Shiller, A.M., 1981. Calculating the oceanic CO_2 increase: a need for caution. J. Geophys. Res. 86 (C11), 11083–11088.
Stoll, M.H.C, Rommets, R.W., de Baar, H.J.W., 1993. Effect of selected calculation routines and dissociation constants on the determination of total carbon dioxide in seawater. Deep-Sea Res. I 40 (6), 1307–1322.
Takahashi, T., Sutherland, S.C., Wanninkhof, R., Sweeney, C., Feely, R.A., Chipman, D.W., Hales, B., Friederich, G., Chavez, F., Sabine, C., Watson, A., Bakker, D.C.E., Schuster, A., Metzl, N., Yoshikawa-Inoue, H., Ishii, M., Midorikawa, T., Nojiri, Y., Koertzinger, A., Steinhoff, T., Hoppema, M., Olafsson, J., Arnarson, T.S., Tilbrook, B., Johannessen, T., Olsen, A., Bellerby, R., Wong, C.S., Delille, B., Bates, N.R., de Baar, H.J.W., 2009. Climatological mean and decadal change in surface ocean pCO_2, and net sea–air CO_2 flux over the global oceans. Deep-Sea Res. II 56, 554–577.
Tanhua, T., Biastoch, A., Körtzinger, A., Lüger, H., Böning, C., Wallace, D.W.R., 2006. Changes of anthropogenic CO_2 and CFCs in the North Atlantic between 1981 and 2004. Global Biogeochem. Cycles 20, GB4017.
Tanhua, T., Körtzinger, A., Friis, K., Waugh, D.W., Wallace, D.W.R., 2007. An estimate of anthropogenic CO_2 inventory from decadal changes in oceanic carbon content. Proc. Natl. Acad. Sci. 104, 3037–3042.
Tanhua, T., Waugh, D.W., Wallace, D.W.R., 2008. Use of SF_6 to estimate anthropogenic CO_2 in the upper ocean. J. Geophys. Res. 113, C04037.
Tanhua, T., van Heuven, S., Key, R.M., Velo, A., Olsen, A., Schirnick, C., 2010. Quality control procedures and methods of the CARINA database. Earth Syst. Sci. Data 2, 35–49.
Touratier, F., Goyet, C., 2004a. Definition, properties, and Atlantic Ocean distribution of the new tracer TrOCA. J. Mar. Syst. 46, 169–179.
Touratier, F., Goyet, C., 2004b. Applying the new TrOCA approach to assess the distribution of anthropogenic CO_2 in the Atlantic Ocean. J. Mar. Syst. 46, 181–197.
Touratier, F., Azouzi, L., Goyet, C., 2007. CFC-11, $\Delta^{14}C$ and ^3H tracers as a means to assess anthropogenic CO_2 concentrations in the ocean. Tellus 59B, 318–325.
van Heuven, S., Pierrot, D., Lewis, E., Wallace, D.W.R., 2009. MATLAB Program Developed for CO_2 System Calculations, ORNL/CDIAC-105b. Carbon Dioxide Information Analysis Center. Oak Ridge National Laboratory, US Department of Energy, Oak Ridge, Tennessee.
Vázquez-Rodríguez, M., Touratier, F., Lo Monaco, C.L., Waugh, D.W., Padin, X., Bellerby, R.G.J., Goyet, C., Metzl, N., Ríos, A., Perez, F., 2009. Anthropogenic carbon distributions in the Atlantic Ocean: data-based estimates from the Arctic to the Antarctic. Biogeosciences 6, 439–451.
Walker, S., Weiss, R., Salameh, P., 2000. Reconstructed histories of the annual mean atmospheric mole fractions for the halocarbons CFC-11 CFC-12, CFC-113, and carbon tetrachloride. J. Geophys. Res. 105, 14285–14296.
Wallace, D.W.R. (Ed.), 1995. Monitoring Global Ocean Carbon Inventories. OOSDP Background Report No. 5. Texas A&M University, College Station, Texas, USA.
Wanninkhof, R., Doney, S., Peng, T., 1999. Comparison of methods to determine the anthropogenic CO_2 invasion into the Atlantic Ocean. Tellus 51B, 511–530.
Waugh, D.W., Hall, T.M., McNeil, B.I., Key, R., Matear, R.J., 2006. Anthropogenic CO_2 in the oceans estimated using transit time distributions. Tellus 58B, 376–389.
Weiss, R., 1970. The solubility of nitrogen, oxygen and argon in water and seawater. Deep-Sea Res. 17, 721–735.
Yool, A., Oschlies, A., Nurser, A.J.G., Gruber, N., 2010. A model-based assessment of the TrOCA approach for estimating anthropogenic carbon in the ocean. Biogeosciences 7, 723–751.